Cellular and Molecular Life Sciences (2022) 79:375
https://doi.org/10.1007/s00018-022-04404-0

ORIGINAL ARTICLE

Mitochondrial FAD shortage in SLC25A32 deficiency affects folate-mediated one-carbon metabolism

Min-Zhi Peng[1] · Yong-Xian Shao[1] · Xiu-Zhen Li[1] · Kang-Di Zhang[1] · Yan-Na Cai[1] · Yun-Ting Lin[1] · Min-Yan Jiang[1] · Zong-Cai Liu[1] · Xue-Ying Su[1] · Wen Zhang[1] · Xiao-Ling Jiang[1] · Li Liu[1]

Received: 21 February 2022 / Revised: 6 May 2022 / Accepted: 27 May 2022 / Published online: 21 June 2022

Abstract

The SLC25A32 dysfunction is associated with neural tube defects (NTDs) and exercise intolerance, but very little is known about disease-specific mechanisms due to a paucity of animal models. Here, we generated homozygous (*Slc25a32*$^{Y174C/Y174C}$ and *Slc25a32*$^{K235R/K235R}$) and compound heterozygous (*Slc25a32*$^{Y174C/K235R}$) knock-in mice by mimicking the missense mutations identified from our patient. A homozygous knock-out (*Slc25a32*$^{-/-}$) mouse was also generated. The *Slc25a32*$^{K235R/K235R}$ and *Slc25a32*$^{Y174C/K235R}$ mice presented with mild motor impairment and recapitulated the biochemical disturbances of the patient. While *Slc25a32*$^{-/-}$ mice die in utero with NTDs. None of the *Slc25a32* mutations hindered the mitochondrial uptake of folate. Instead, the mitochondrial uptake of flavin adenine dinucleotide (FAD) was specifically blocked by *Slc25a32*$^{Y174C/K235R}$, *Slc25a32*$^{K235R/K235R}$, and *Slc25a32*$^{-/-}$ mutations. A positive correlation between SLC25A32 dysfunction and flavoenzyme deficiency was observed. Besides the flavoenzymes involved in fatty acid β-oxidation and amino acid metabolism being impaired, *Slc25a32*$^{-/-}$ embryos also had a subunit of glycine cleavage system—dihydrolipoamide dehydrogenase damaged, resulting in glycine accumulation and glycine derived-formate reduction, which further disturbed folate-mediated one-carbon metabolism, leading to 5-methyltetrahydrofolate shortage and other folate intermediates accumulation. Maternal formate supplementation increased the 5-methyltetrahydrofolate levels and ameliorated the NTDs in *Slc25a32*$^{-/-}$ embryos. The *Slc25a32*$^{K235R/K235R}$ and *Slc25a32*$^{Y174C/K235R}$ mice had no glycine accumulation, but had another formate donor—dimethylglycine accumulated and formate deficiency. Meanwhile, they suffered from the absence of all folate intermediates in mitochondria. Formate supplementation increased the folate amounts, but this effect was not restricted to the *Slc25a32* mutant mice only. In summary, we established novel animal models, which enabled us to understand the function of SLC25A32 better and to elucidate the role of SLC25A32 dysfunction in human disease development and progression.

Keywords Riboflavin-responsive exercise intolerance · Multiple acyl-coenzyme A dehydrogenation deficiency · Dimethylglycine dehydrogenase · Serine metabolism · Clubfoot · Hypoplasia of fibulae

Introduction

Riboflavin-responsive exercise intolerance (RREI, #616839) is an autosomal recessive disorder caused by mutations in the *SLC25A32* gene (#138480). It was discovered in 2016, and several cases have been reported. These cases all have disease onset at childhood and present with neuromuscular phenotypes, such as exercise intolerance, ataxia, myoclonus, dysarthria, and dysphagia [1, 2], or with only hypoketotic and hypoglycemia but no neuromuscular complications [3]. Metabolites analysis reveals biochemical features of multiple acyl-coenzyme A dehydrogenation deficiency (MADD). Supplementation with riboflavin, the precursor of flavin

Min-Zhi Peng, Yong-Xian Shao and Xiu-Zhen Li: Co-first authors.

✉ Wen Zhang
zhw2001zhw@163.com

✉ Xiao-Ling Jiang
JiangGenetics@126.com

✉ Li Liu
liliuchina@qq.com

[1] Department of Genetics and Endocrinology, Guangzhou Women and Children's Medical Center, the Affiliated Hospital of Guangzhou Medical University, 9 Jinsui Road, Guangzhou, China

adenine dinucleotide (FAD), improves patients' clinical symptoms.

The *SLC25A32* gene locates on chromosome 8q22.3 and contains seven exons. It encodes a 35 kDa protein SLC25A32 [4] and is ubiquitously expressed in all tissues [5]. SLC25A32 was proposed as a mitochondrial FAD transporter according to its ability to functionally complement the *FLX1*-mutated yeast strain with mitochondrial FAD transport defect [6]. The pathogenesis of RREI was considered caused by the mitochondrial FAD transport defect, which reduced the activities of mitochondrial flavoproteins involved in fatty acid β-oxidation (FAO) and the respiratory chain [1]. However, earlier studies suggested that SLC25A32 was a mitochondrial folate transporter [4, 7]. Variation in *SLC25A32* SNP rs17803441 was found to be associated with lower 5-methyltetrahydrofolate (CH3-THF) concentrations in human red blood cells [8]. Recently, biallelic loss of function variants in the *SLC25A32* gene had been identified in the human fetus with neural tube defects (NTDs), and *Slc25a32* gene trapped knock-out mice also presented with cranial NTDs in the embryonic stage [9]. It is well known that the folate-mediated one-carbon metabolism (FOCM) abnormality is the most critical modifier of risk associated with neural tube closure [10, 11].

In clinic, we identified a patient who carried novel *SLC25A32* point mutations and presented with muscle weakness and intractable clubfeet. Neither riboflavin supplementation nor surgery blocked the development of clubfeet. Clubfoot is usually a secondary manifestation of spina bifida, distal arthrogryposis, congenital myotonic dystrophy, etc. Its etiopathogenesis is still unknown regardless of its long-lasting recognition [12], of which spina bifida is a type of NTD. The reported RREI patients [1–3] had similar clinical manifestations, biochemical features, and responses to riboflavin supplementation as MADD patients. However, clubfoot is not observed in MADD patients, although MADD patients with the most severe symptoms also had congenital anomalies, such as dysmorphic facial features, large cystic kidneys, hypospadias and chordee in males, and neuronal heterotopias [13]. The different phenotypes suggest distinct pathogenic mechanisms or common underlying pathogenesis for the two inborn errors. The complexity of the disease prompted us to reconsider the etiology and treatment strategy of RREI. In this study, we first reviewed the clinical history of the case and performed a morphology study and neuropsychological evaluation for the patient. By mimicking the mutations identified in our patient, we generated multiple mice models with variable degrees of SLC25A32 dysfunctions to study the pathophysiology of RREI. Our results advanced our understanding of the relationship between the *Slc25a32* mutant and NTDs, and how SLC25A32 dysfunction affected mitochondrial flavoenzymes. New findings suggested potential therapeutic intervention for patients suffering from mitochondrial FAD deficiency.

Materials and methods

Study approval

This study was performed in line with the principles of the Declaration of Helsinki. The ethics committee of Guangzhou Women and Children's Medical Center authorized this study, and the Institutional Animal Care and Use Committee of Guangzhou Medical University approved the animal studies. Informed consent was obtained from the patient and her guardian.

Generation of *Slc25a32* mutant mice models

Human *SLC25A32 c.521A > G* (*p.Y174C*) and *c.704A > G* (*p.K235R*) are conserved to mouse *Slc25a32* (NM_172402) *c.521A > G* (*p.Y174C*) and *c.704A > G* (*p.K235R*), respectively. CRISPR/Cas9 technology was utilized to generate the mouse mutants with the corresponding missense mutations. The sgRNAs used for generating the *p.Y174C* and *p.K235R* mouse mutants were TATAAATATGAAGGTGTGCGTGG (matching the forward strand of *Slc25a32*), and ATACGG GTATGTTGCTGCTACCGG (matching the reverse strand of *Slc25a32*), respectively (PAM sequence was underscored). The oligo donors for generating the *p.Y174C* and *p.K235R* mouse mutants were GGTGTTGCTAGCCCTTCACAG AGACAGTATAAAGGAATGTTTGATGCACTTGTGAAA ATATGTAAATATGAAGGTGTGAGAGGATTATACAAG GTAACAAATTATCATGAATATATTTTGAGTACTGGA AATC and ATCCTGCTTGTGTTCTCATTTTAGAGT ACAGCAGAATACATCTCTGTCGCAGCGCTATCCAGA ATATTTGCGGTAGCAGCAACATACCCGTATCAGGTT GTGAGAGCCCGCCTTCAGGATCAG, respectively. The *p.Y174C* (*c.521A > G*, TAT to TGT) mutation in donor oligo was introduced into exon 4, and the *p.K235R* (*c.704A > G*, AAA to AGA) mutation in donor oligo was introduced into exon 6, by homology-directed repair. Silent mutations *p.R180=*, CGT to AGA and *c.714C > G*, GCC to GCG were co-introduced for *p.Y174C* and *p.K235R* mutants, respectively, to prevent the binding and re-cutting of the sequence by sgRNA after homology-directed repair.

The Cas9 mRNA, sgRNA, and oligo donor were co-injected into fertilized C57BL/6 eggs. Founders with the expected mutation were identified by sequencing the PCR amplicons of tail DNA. Primers for identifying *p.Y174C* mutation were: forward 5′-GATCACGTGGGCCTTCTT TATGC-3′ and reverse 5′-TTTACACCAATGAAGACACAG CTTATGG-3′. Primers for identifying *p.K235R* mutation were: forward 5′-AGAACCCCATATTAAATAGACCTC

GTG-3′ and reverse 5′-AAATGAGGAAATCAGGCTTCA GAGAC-3′.

The mutant mice were crossed to wild-type C57BL/6 mice for at least three generations to eliminate potential off-targeting mutations. Potential off-targeting sites were predicted using CCTOP (https://cctop.cos.uni-heidelberg.de/), and the whole *Slc25a32* coding region and flanking sequences were sequenced for potential off-targeting mutations. Specifically, in the generation of the *p.Y174C* mouse mutant, we obtained a mutant mouse with an additional *c.552G>A* (AAG to AAA) mutation at the end of the fourth exon. This mutation interfered with the splicing of *Slc25a32* and did not produce detectable normal transcripts. This mouse mutant was kept and used as a "knock-out" allele in this study. Genotyping was performed by sequencing the PCR amplicons of tail or embryo amnion, and the primers were: forward 5′-AATATGGATTGCATGAAACAGTAC C-3′ and reverse 5′-TGTACTCTGTAGTCTTGGATGGGA A-3′.

Four types of mating with $Slc25a32^{Y174C/+} \times Slc25a32^{Y174C/+}$, $Slc25a32^{K235R/+} \times Slc25a32^{K235R/+}$, $Slc25a32^{Y174C/+} \times Slc25a32^{K235R/+}$, and $Slc25a32^{+/-} \times Slc25a32^{+/-}$ were set up to obtain homozygous ($Slc25a32^{Y174C/Y174C}$ and $Slc25a32^{K235R/K235}$) and compound heterozygous ($Slc25a32^{Y174C/K235R}$) knock-in and homozygous ($Slc25a32^{-/-}$) knock-out mice. Wild-type (WT, $Slc25a32^{+/+}$) mice or embryos were used as controls. All mice were housed in an SPF facility with a 12-h light/dark cycle and allowed access to water and mouse chow *ad libitum*.

Collection of tissues and embryos

Mice aged 2–3 months were killed by cervical dislocation, and skeletal muscle and brain tissues were isolated rapidly, then chilled in liquid nitrogen or minced into small pieces for mitochondria isolation. Embryos at embryonic day 11.5 (E11.5) were dissected from dams and chilled in liquid nitrogen or pooled by genotype for mitochondria isolation.

Isolation of mitochondria

Mitochondria used for this study were isolated from skeletal muscle using the differential centrifugation method, according to the published protocol [14]. Several E11.5 $Slc25a32^{-/-}$ embryos were pooled as one sample for mitochondria isolation using the same protocol for isolating mice liver mitochondria [14]. The purity of mitochondria was examined by Janus green B staining, light microscopic examination, and immunoblot analyses of markers for individual subcellular organelles, as previously described [15].

Slc25a32 gene mRNA expression

Total mRNA was isolated from skeletal muscle or embryo using TRIzol® Reagent (ambion®, Life technologies, USA) according to the manufacturer's protocol. cDNA was synthesized by the PrimeScript™ RT Master Mix kit (TAKARA, Japan). For the mouse mutants with *Slc25a32* missense mutations, real-time quantitative PCR (Q-PCR) was performed to determine the abundance of *Slc25a32* mRNAs by using the primers 5′-ATGGGTGACGAAAAC TCGCCTT-3′ and 5′-CGCACCATGTGATGTTCCAAA-3′ on a LightCycler® 480II system (Roche, Switzerland) with SYBR® Premix Ex Taq™ II (TAKARA, Japan) reagent. GAPDH was used as the loading control. For the $Slc25a32^{-/-}$ mice, primers located on exon 2 and 7 of *Slc25a32* (5′-AATATGGATTGCATGAAACAGTACC-3′ and 5′-TCCACCGATGCCTTCTTTCC-3′) were used to amplify a 678-bp amplicon of the *Slc25a32* coding region. The amplicons were then separated by gel electrophoresis and purified for DNA sequence analysis.

Determination of proteins by capillary immunoassay (simple western)

Total protein was extracted from skeletal muscle or embryos with RIPA lysis buffer (P0013C, Beyotime, China) according to the protocol from the manufacturer. The concentrations were determined using BCA Protein Assay Kit (BCA1, Sigma-Aldrich). A capillary-based automated Simple Western system (Wes, ProteinSimple, San Jose, CA, USA) measured the amounts of SLC25A32 and nine mitochondrial flavoenzymes in the lysates. The Wes 12–230 kDa separation module, 8×25 capillary cartridges (SM-W004), was used. Specifically, the lysate was diluted with sample buffer from the kit to 1.25×of the desired final concentration, then mixed with the Master Mix from the kit. The mixture was denatured at 95 °C for 5 min. 3 µL of the denatured sample was loaded to a capillary. Primary antibodies were purchased and diluted with antibody dilution II solution from the kit before use: anti-SLC25A32 (orb37248, Biorbyt, Cambridge, UK; 1:50 dilution), anti-ACADS (ab156571, Abcam, Cambridge, UK; 1:100 dilution), anti-ACADM (ab92461, Abcam; 1:50 dilution), anti-ACADVL (ab155138, Abcam; 1:50 dilution), anti-ACAD8 (A68138, Epigentek, NY, USA; 1:50 dilution), anti-ACADSB (13122-1-AP, Proteintech, Rosemont, USA; 1:50 dilution), anti-IVD (10822-1-AP, Proteintech; 1:100 dilution), anti-ETFA (12262-1-AP, Proteintech; 1:50 dilution), anti-ETFB (#43,776, Signalway Antibody; 1:50 dilution), anti-ETFDH (11109-1-AP, Proteintech; 1:100 dilution), anti-GCSH (NBP1-85842, Novus Biologicals, CO, USA; 1:50 dilution), anti-glycine decarboxylase (ab232989, Abcam; 1:50 dilution), anti-DLD (16431-1-AP, Proteintech; 1:200 dilution), and anti-AMT (orb374296, Biorbyt; 1:100

dilution). Anti-GAPDH (AF7021, Affinity, OH, USA), anti-α-tubulin (11224-1-AP, Proteintech), or anti-HSP60 (15282-1-AP, Proteintech) was chosen as loading control according to the molecular weight of the target protein. The target protein and its loading control were multiplexed in the same capillary by mixing the primary antibody with the loading control antibody. Goat anti-rabbit or anti-mouse IgG secondary antibody from the kit was used. The Wes system ran with the default program (Separation time 30 min, Separation voltage 375 V, Antibody diluent time 5 min, primary antibody incubation time 30 min, secondary antibody incubation time 30 min). Compass software (ProteinSimple) was used to visualize virtual gels. The relative protein quantification was obtained by normalizing the signal of the target protein against the signal of its loading control.

Analysis of mitochondrial uptake of folates and flavins

About 200 µg of mitochondria was resuspended in the MiRO5 respiration medium (110 mmol/L sucrose, 20 mmol/L HEPES, 10 mmol/L KH_2PO4, 20 mmol/L taurine, 60 mmol/L K-lactobionate, 3 mmol/L $MgCl_2$, 0.5 mmol/L EGTA, and 1 g/L fatty acid-free BSA, adjusted pH to 7.2 with KOH), according to the published protocol [16]. The assay was initiated by adding stable isotope-labeled [$^{13}C_5$]-FAD, [$^{13}C_4$, $^{15}N_2$]-riboflavin (Rf), [^{15}N]-folate (FA), or 5-formyl-tetrahydrofolate (CHO-THF) to a final concentration of 10 µmol/L. The suspensions were incubated at 37 °C for a specific time, and mitochondria were pelleted by centrifugation (4 °C, 14,000 *g* for 2 min) after the reaction. The pellet was washed twice with ice-cold mitochondrial isolation buffer. The mitochondria absorbed [$^{13}C_5$]-FAD, [^{15}N]-folate, [$^{13}C_4$,$^{15}N_2$]-riboflavin, and CHO-THF were extracted in ice-cold 4% perchloric acid and analyzed by a liquid chromatography–tandem mass spectrometry (LC–MS/MS) (Shimadzu Ultrahigh Pressure Nexera chromatograph system (Kyoto, Japan) interfaced to a Sciex QTRAP 5500 + mass spectrometer (AB Sciex LLC, Framingham, MA, USA)) according to the published protocols [17, 18].

Metabolites analysis

Nitrogen chilled skeletal muscle and whole-brain tissues were first pulverized by CryoGrinder™ System and then homogenized in PBS by sonication. Embryos were homogenized in PBS by sonication directly. Homogenates were centrifuged to remove debris (4 °C, 15,000 *g* for 20 min), and the supernatants were used for metabolite analysis. An aliquot of each sample was removed for total protein quantification. Analysis of acylcarnitine, amino acids, organic acids, DMG, and formate was carried out according to the published protocols [19–22] using the LC–MS/MS system (Shimadzu Ultrahigh Pressure Nexera chromatograph system interfaced to an AB Sciex 3200 Q TRAP mass spectrometer (Foster City, CA, USA)), or a gas chromatography–mass spectrometry system (GC–MS, Agilent 5975GC-4890MS, USA) [23].

Flavoenzyme activity assays

The enzymatic activities of short/branched-chain acyl CoA- (SBCAD), isovaleryl CoA- (IVD), isobutyryl CoA- (IBD), glutaryl CoA- (GCDH), short-chain- (SCAD), medium-chain- (MCAD), and very-long-chain acyl-CoA dehydrogenases (VLCAD), in skeletal muscle homogenates, were determined based on the published methods [24, 25]. The mitochondrial dihydrolipoamide dehydrogenase (DLDH) activity was measured by a spectrophotometer (BioTek Synergy HTX) according to the protocol described in Ref. [26]. The relative activity of each enzyme in *Slc25a32* mutant mice was expressed as a ratio compared to the activity levels of the WT mice at the reaction system without exogenous FAD supplementation.

Mitochondrial formate synthesis assay

Measurement of mitochondrial synthesis of formate from glycine was carried out as described previously [27]. Briefly, mitochondria were resuspended in the incubation buffer (pH 7.4) consisting of 140 mmol/L KCl, 5.0 mmol/L HEPES, 4.0 mmol/L KPO_4, 2.5 mmol/L $MgCl_2$, 1.5 mmol/L EDTA, and 1.6 mmol/L ADP. The reaction was initiated by adding 1.0 µL of 0.5 mol/L [1, 2-$^{13}C_2$]-glycine solution to 20 µg of mitochondria. Samples were incubated at 37 °C for 24 h. The generated [^{13}C]-formate was derivatized along with its internal standard [^{13}C, D]-formate by *o*-benzylhydroxylamine and analyzed by the LC–MS/MS system.

Statistics

All results were presented as mean values ± standard error of the mean (SEM). Statistical analysis was performed using SPSS. The two-tailed unpaired Student's *t* test was used to compare two groups. $P < 0.05$ was considered significant.

Results

An RREI case with novel *SLC25A32* mutations

A 7-year-old female patient came to our department complaining of dyspnea, fatigue, and growth retardation (height 108 cm (−3 SD), weight 18 kg (− 2 SD to − 1 SD)). Blood gas analysis demonstrated that she suffered from acidosis

with the pH at 7.276 (ref. 7.31–7.41) and lactic acid elevated to 10.7 mmoL/L (ref. 0.9–1.7 mmoL/L). Plasma metabolite analysis revealed a MADD-like biochemical profile with dimethylglycine (DMG), sarcosine, and multiple acylcarnitines accumulation (Fig. 1A). The patient was diagnosed with MADD and immediately received a low protein diet and oral supplementation of riboflavin and L-carnitine. After a 2-week treatment, the patient's dyspnea disappeared, and the biochemical abnormality ameliorated. From then on, the patient received riboflavin (30 mg P.O. tid) and L-carnitine (1 g P.O. qid) supplementation with a normal diet. Now, the patient is a 20-year-old with nearly normal growth (height 155 cm (-1SD); weight 58 kg (mean 51 kg)).

Before coming to our department, the patient was found to be unwilling to walk after suffering from influenza at 1.6-year-old. Her feet developed to equinovarus and talipes cavus progressively. The right foot was more severe than the left one initially. She underwent orthopedic surgery to correct her right leg at 5.5-year-old, and the surgery was successful (Fig. 1B). Unexpectedly, the deformity of her left leg deteriorated gradually even under riboflavin treatment, and she underwent her second orthopedic surgery at 9-year-old. However, this operation did not improve her symptom. Instead, it relapsed: the forefoot adducted, the talus broadened and was less convex, the the calcaneus became shorter, wider, and angulated medially, and the lateral angle of the talocalcaneal diminished (Fig. 1B).

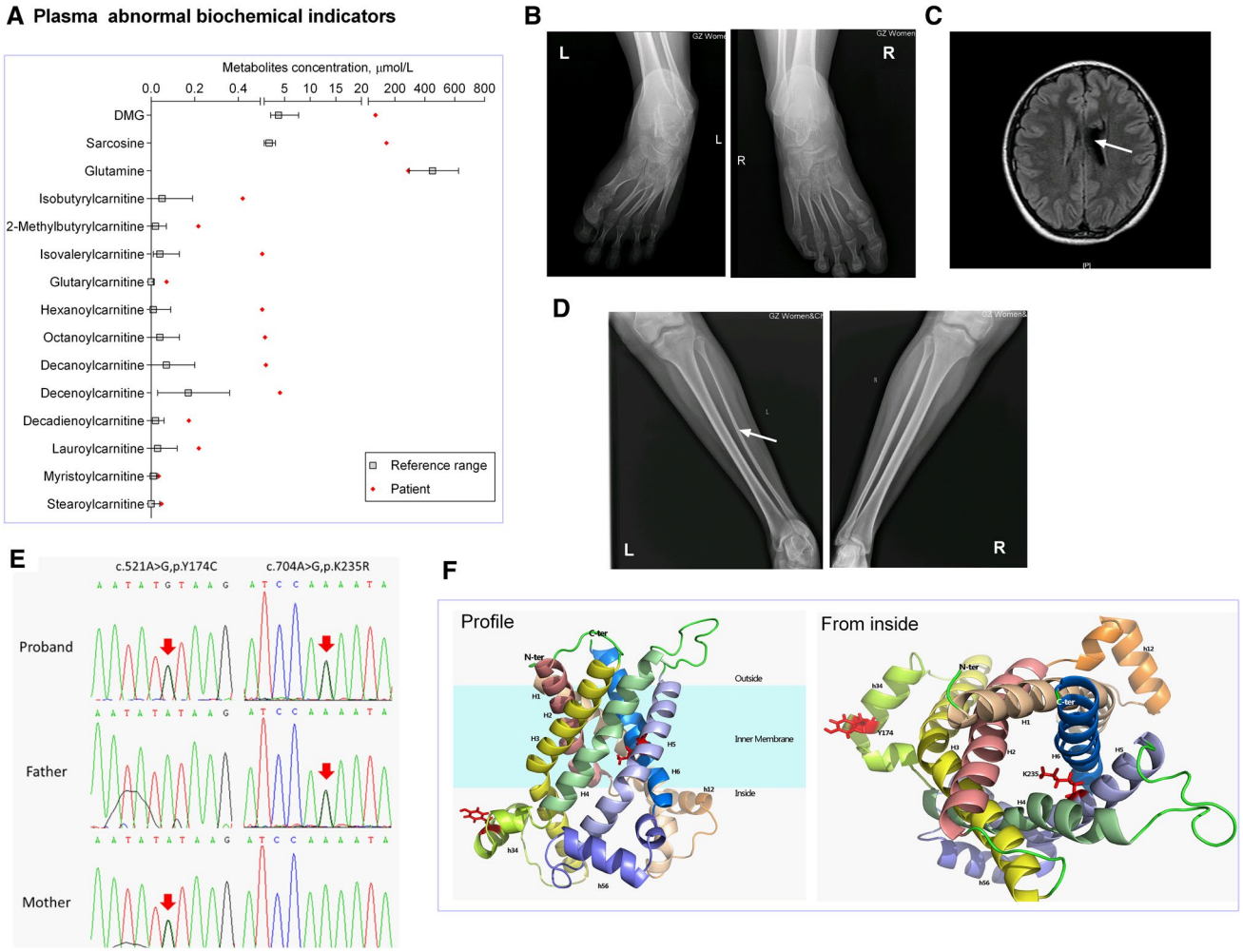

Fig. 1 A RREI case with novel mutations in the *SLC25A32* gene. **A** Metabolic analysis of plasma amino acids and acylcarnitines suggested MADD. **B** X-ray imaging of the feet of the patient after orthopedic surgery. The left clubfoot relapsed after surgery. **C** Brain MRI revealed that the left lateral ventricle of the patient broadened slightly. **D** X-ray imaging showed that the left fibula of the patient was abnormally slim. **E** Compound heterozygous mutations in *SLC25A32* were identified from the patient, and testing for the mutations in parental samples confirmed that the unaffected parents were heterozygous for the mutations. **F** Homology modeling analysis using the mitochondrial ADP/ATP carrier (PDB ID: 6GCI) as the template predicted that K235 was located at the substrate-binding pocket and the Y174 at the second matrix loops facing the mitochondrial matrix

A morphology study was performed to investigate the etiology of lower extremity weakness and clubfeet of the patient. The magnetic resonance imaging (MRI) revealed an enlarged left lateral ventricle (Fig. 1C). Electromyography found no abnormality in the peroneal nerve, and the signal transmission between peroneal nerves to muscle was fluent. X-ray imaging of tibiofibular bones showed slender fibulae, and the left one was more severely affected than the right one, suggesting fibulae hypoplasia (Fig. 1D).

The patient then underwent a comprehensive neuropsychological evaluation at 15.8-year-old to identify whether neurologic impairment was involved. The gross motor function measure (GMFM) was carried out at first, and the results showed that the patient had scores in the D (standing) and E (walking, running, and jumping) domains at 90% and 60% of the total domain scores, respectively, indicating an inferior motor function in these domains. The intelligence test (Wechsler Intelligence Scale for Children IV) demonstrated that the patient's intelligence was at the borderline with a full-scale intelligence quotient of 71. In addition, her auditory- and visual-working memory function had mild to moderate defects with scores of 9 and 6, respectively.

MADD is commonly caused by defects in electron transportation due to variants in the *ETFA*, *ETFB*, or *ETFDH* genes. However, Sanger sequencing found no mutation in these genes of the patient. Whole-exome sequencing was then performed, and compound heterozygous mutations in *SLC25A32* were identified: *c.521A > G* (p.Y174C) and *c.704A > G* (p.K235R) (Fig. 1E), which were located at the fourth and sixth exon of *SLC25A32*, respectively. Testing the mutations in parental samples confirmed that the unaffected parents were heterozygous for the mutations. Neither variant was listed in the gnomAD database. Both affected residues were highly conserved across species (the p.Y174 conserved up to *Drosophila melanogaster*, and the p.K235 conserved up to *Saccharomyces cerevisiae*). Protein structure homology modeling analysis using the mitochondrial ADP/ATP carrier (PDB ID: 6GCI) as the template predicted that K235 was located at the substrate-binding pocket and Y174 at the second matrix loops facing the mitochondrial matrix (Fig. 1F). Both variants were likely to damage the SLC25A32 protein by 4 of 4 in silico tools—Protein Variation Effect Analyzer (PROVEAN), Sorting Intolerant from Tolerant (SIFT), PolyPhen, and MutationTaster.

In summary, the phenotypes of our patient include riboflavin-responsive dyspnea, growth retardation, muscle weakness, and exercise intolerance, but riboflavin-unresponsive clubfeet, hypoplasia of fibulae, and mild neuropsychological abnormality. We wondered whether mitochondrial folate transport deficiency was involved in RREI and whether the stubborn clubfeet resulted from folate transport defect. To answer these questions, we performed this study.

Various phenotypes were observed in mice carrying different *Slc25a32* mutations.

The homozygous ($Slc25a32^{Y174C/Y174C}$ and $Slc25a32^{K235R/K235}$) and compound heterozygous ($Slc25a32^{Y174C/K235R}$) knock-in mice were born with the expected Mendelian ratio. No genotype effect was observed on birth weight, neonatal growth, or adult weight. Clubfoot was not observed in mice models after examining the gait of 40 $Slc25a32^{Y174C/Y174C}$, 67 $Slc25a32^{K235R/K235R}$, and 39 $Slc25a32^{Y174C/K235R}$ mice. Q-PCR revealed the $Slc25a32^{Y174C/Y174C}$ mice, but not the $Slc25a32^{K235R/K235R}$ and $Slc25a32^{Y174C/K235R}$ mice, showed significantly reduced *Slc25a32* mRNA expression in muscle (Fig. 2A). Consistently, the immunoblot assay showed reduced SLC25A32 protein amounts in $Slc25a32^{Y174C/Y174C}$ muscle (Fig. 2B). To assess whether the mutant mice had motor impairment as our patient had, we tested the muscle strength, exercise coordination, and anti-fatigue capacity of mice by performing hanging wire test, rotarod test, and forced swimming test (FST), following the published protocols [28–30]. Adult mice aged 2–3 months (weighed 18.6 ± 1.6 g) were used. The times hanging on the wire were shorter for the $Slc25a32^{Y174C/K235R}$ and $Slc25a32^{K235R/K235R}$ mice than for their WT littermates, though the difference did not reach significance (Fig. 2C). The $Slc25a32^{K235R/K235R}$ mice also performed worse in the rotarod test and FST than their WT littermates (Fig. 2D). The motor function of $Slc25a32^{Y174C/Y174C}$ mice was comparable with their WT littermates.

No $Slc25a32^{-/-}$ pup was born from the $Slc25a32^{+/-} \times Slc25a32^{+/-}$ mating. Embryos collected at the embryonic day of 11.5 (E11.5, the post-neurulation-stage in normal mouse embryos) showed that 89.5% ($n = 94$) of $Slc25a32^{-/-}$ embryos had NTDs with exencephaly or craniorachischisis phenotypes, and the rest ($n = 11$) had normal neural tube closure but severe growth retardation (Fig. 2E). Sequencing of DNA amplicons of $Slc25a32^{-/-}$ embryo amnions revealed that the point mutation (TAT to TGT) and the silent mutation (AAG to AAA) were co-introduced successfully in both strands of the *Slc25a32* gene (Fig. 2F, G). The reverse transcription PCR (RT-PCR) using primers located on exon 2 and 7 of the *Slc25a32* gene showed that a 678 bp cDNA fragment observed in WT embryo was absent in $Slc25a32^{-/-}$ embryos. Instead, fragments at 517 bp

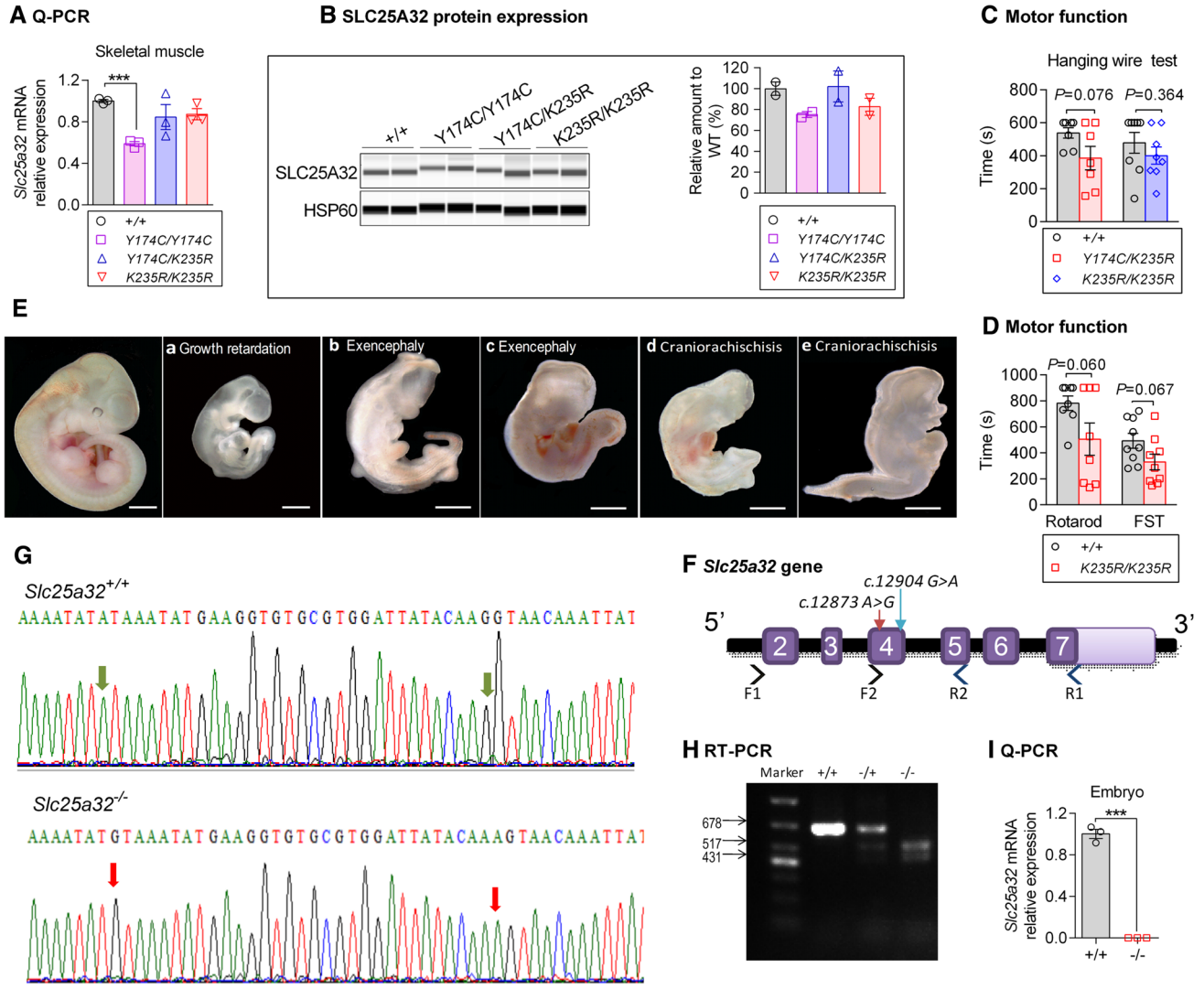

Fig. 2 Characterization of mouse models with *Slc25a32* gene mutants. **A** *Slc25a32* mRNA expression in skeletal muscle of *Slc25a32* mutant mice ($n=3$). A significant difference was observed between $Slc25a32^{+/+}$ and $Slc25a32^{Y174C/Y174C}$ mice. **B** SLC25A32 protein in skeletal muscle of *Slc25a32* mutant mice ($n=2$). **C** The hanging wire test showed that the times hanging on the wire were shorter for the $Slc25a32^{Y174C/K235R}$ and $Slc25a32^{K235R/K235R}$ mice than for $Slc25a32^{+/+}$ mice, but the difference did not reach significance ($n=7$–8). **D** The rotarod test and FST revealed that the $Slc25a32^{K235R/K235R}$ mice performed worse than their WT littermates, but the difference did not reach significance ($n=8$). **E** Various NTDs were observed in E11.5 $Slc25a32^{-/-}$ embryos. a, No NTDs but growth retardation; b, c: exencephaly; d, e: craniorachischisis (scale bars represent 1 mm). **F** Generation of the *Slc25a32* knock-out mouse model using the CRISPR/Cas9 system. Two mutation sites (*c.12873 A>G, c.12904 G>A*) in donor oligo were introduced into exon 4 by homology-directed repair. The primers used for RT-PCR and Q-PCR were indicated. **G** Sequencing of DNA amplicons of $Slc25a32^{+/+}$ and $Slc25a32^{-/-}$ embryo amnions. The point mutation (TAT to TGT) and a silent mutation (AAG to AAA) were co-introduced in both strands of *Slc25a32* gene for $Slc25a32^{-/-}$ embryo. **H** RT-PCR for *Slc25a32* mRNA expression in E11.5 embryos using primers F1-R1 showed that a 678 bp cDNA fragment observed in $Slc25a32^{+/+}$ embryo was absent in $Slc25a32^{-/-}$ embryos. Instead, fragments at 517 bp and 431 bp were presented in $Slc25a32^{-/-}$ embryos. **I** Q-PCR for *Slc25a32* mRNA expression in E11.5 embryos using primers F2-R2 showed undetectable *Slc25a32* transcripts in $Slc25a32^{-/-}$ embryos ($n=3$). *n* represents biologically independent replicates. Data are mean ± SEM. The *P* values were determined by an unpaired, two-tailed Student's *t* test. ***$P<0.001$ versus $Slc25a32^{+/+}$

and 431 bp were presented (Fig. 2H). Sequence analysis revealed that the 517 bp and 431 bp fragments were truncated transcripts that lacked exon 4 and both exon 3 and 4, respectively. Q-PCR using primers located on exon 4 and 5 showed no *Slc25a32* mRNA expression in $Slc25a32^{-/-}$ embryos (Fig. 2I).

The SLC25A32 is not a mitochondrial folate transporter, but plays an essential role in FOCM

To investigate whether folate transport deficiency was involved in RREI, we first analyzed the folate profile of mitochondria isolated from the skeletal muscle of mice.

The tetrahydrofolate (THF) and 5, 10-methenyl-tetrahydrofolate (CH-THF) were the primary folate intermediates in mitochondria, accounting for > 90% of the total folate. The *Slc25a32*$^{K235R/K235R}$ mice, but not *Slc25a32*$^{Y174C/Y174C}$ mice, had significantly lower levels of all folate intermediates than the WT mice (Fig. 3A). We further tested the mitochondrial folate uptake rate. The stable isotope-labeled [^{15}N]-FA and CHO-THF were used as substrates. The results showed that neither the uptake of [^{15}N]-FA nor the uptake of CHO-THF was hindered by any of the *Slc25a32* mutants (Fig. 3B), which suggested that mitochondrial folates deficiency in *Slc25a32*$^{K235R/K235R}$ mice was not caused by folate transport defect.

To further clarify whether SLC25A32 was involved in folate transport, we isolated mitochondria from the embryos of *Slc25a32*$^{K235R/K235R}$, *Slc25a32*$^{-/-}$ and their WT siblings to test their ability to uptake [^{15}N]-FA and CHO-THF. The experiment found no deficiency in mitochondrial uptake of folates for *Slc25a32*$^{K235R/K235R}$ and *Slc25a32*$^{-/-}$ embryos (Fig. 3C). Meanwhile, we analyzed

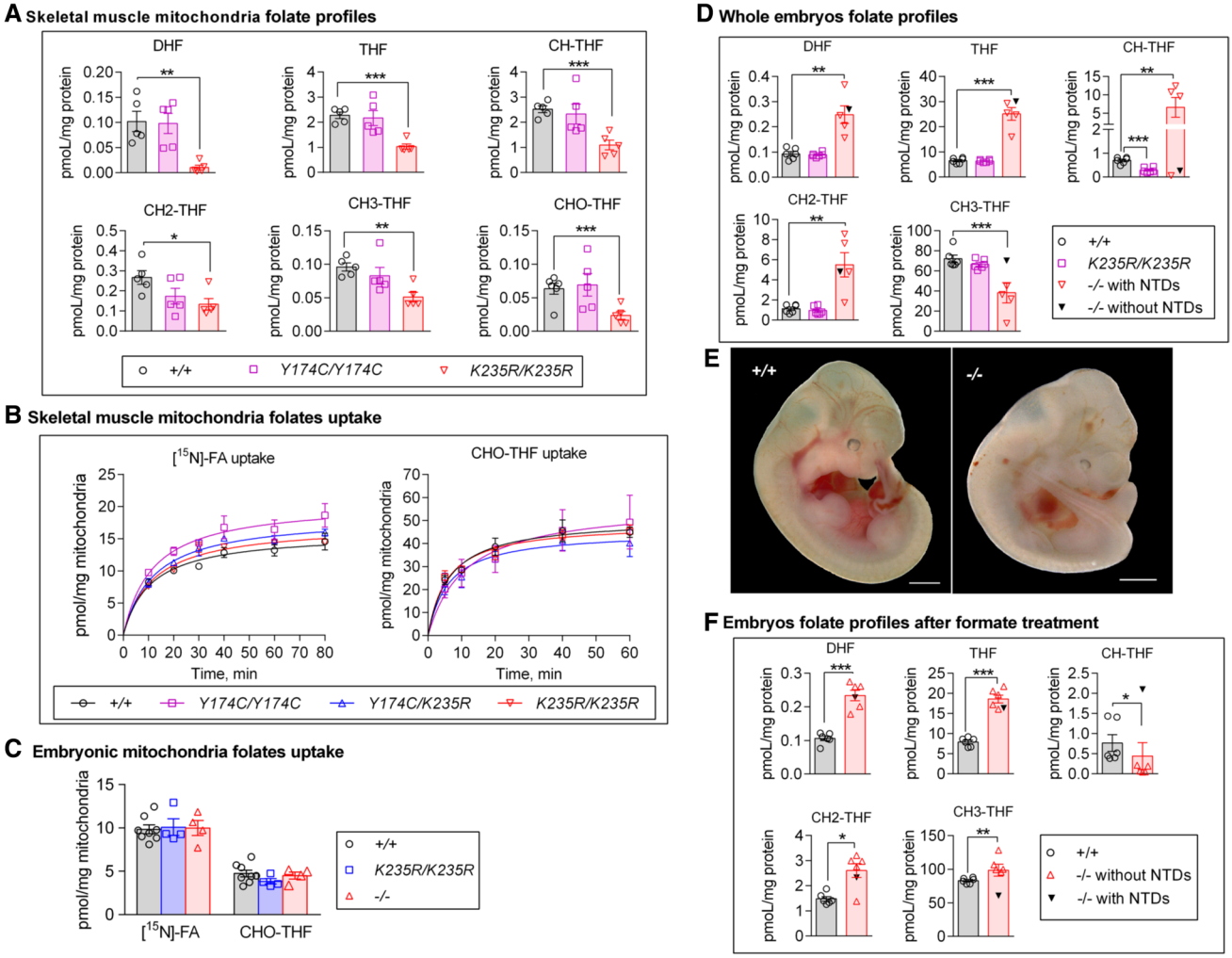

Fig. 3 The *Slc25a32* mutations interrupted folate metabolism. **A** Mitochondrial folate profiles of *Slc25a32* mutant mice ($n=5$). The abundances of all folate intermediates were significantly lower in *Slc25a32*$^{K235R/K235R}$ than in controls. **B** Mitochondria uptake of [^{15}N]-FA and CHO-THF ($n=3$). Mitochondria were isolated from skeletal muscle of *Slc25a32* mutant and WT mice. The folate uptake rates were comparable for *Slc25a32* mutant and WT mice. **C** The mitochondria absorbed [^{15}N]-FA and CHO-THF amounts in 60 min ($n=4$–8). Mitochondria were isolated from *Slc25a32*$^{+/+}$, *Slc25a32*$^{K235R/K235R}$ and *Slc25a32*$^{-/-}$ embryos. The folate uptake amounts were comparable for them. **D** Folate profiles of whole embryos ($n=5$). Different folate profiles were observed in *Slc25a32*$^{K235R/K235R}$, *Slc25a32*$^{-/-}$ with NTDs, *Slc25a32*$^{-/-}$ without NTDs, and *Slc25a32*$^{+/+}$ embryos. **E** Neural tube closure completed in E11.5 *Slc25a32*$^{-/-}$ embryo following maternal sodium formate supplementation (scale bars represent 1 mm). **F** Folate profiles of E11.5 embryos following maternal sodium formate supplementation ($n=6$). Different folate profiles were observed in *Slc25a32*$^{-/-}$ with NTDs, *Slc25a32*$^{-/-}$ without NTDs, and *Slc25a32*$^{+/+}$ embryos. *n* represents biologically independent replicates. Data are mean ± SEM. The *P* values were determined by an unpaired, two-tailed Student's *t* test, $^{*}P<0.05$, $^{**}P<0.01$, $^{***}P<0.001$ versus *Slc25a32*$^{+/+}$ control

the folate profiles of whole embryos. Unlike the mitochondrial folate profile, the whole embryo folate profile had the CH3-THF as the primary folate intermediate, while the level of CHO-THF was too low to be detected. Compared with controls, the *Slc25a32*$^{K235R/K235R}$ embryos had slightly disturbed folate profiles with only CH-THF levels decreased. The *Slc25a32*$^{-/-}$ embryos had thoroughly disturbed folate profiles: the amounts of dihydrofolate (DHF), THF, CH-THF, and 5, 10-methylene THF (CH2-THF) significantly increased, and the amounts of CH3-THF significantly decreased (Fig. 3D). As mentioned above, 10.5% of *Slc25a32*$^{-/-}$ embryos showed normal neural tube closure. We noticed that the *Slc25a32*$^{-/-}$ embryo without NTDs had comparable CH3-THF amount as the WT embryos (Fig. 3D), which differed from the *Slc25a32*$^{-/-}$ embryos with NTDs and suggested a close relationship between CH3-THF and NTDs.

A previous study evidenced that maternal CH3-THF supplementation failed to rescue the NTDs of *Slc25a32* knock-out embryos, but formate could [9]. We repeated the same experiment but used 0.1 mol/L sodium formate instead of calcium formate in the dam's drinking water. We collected 73 embryos from 9 litters, and genotyping revealed that there were 16 *Slc25a32*$^{+/+}$, 41 *Slc25a32*$^{+/-}$, and 16 *Slc25a32*$^{-/-}$ embryos, of which 87.5% of *Slc25a32*$^{-/-}$ embryos completed neural tube closure (Fig. 3E). Analyzing the folate profile again showed that the levels of CH3-THF were significantly higher, and the levels of CH-THF were significantly lower in *Slc25a32*$^{-/-}$ embryos without NTDs than in their WT siblings (Fig. 3F). The levels of DHF, THF, and CH2-THF decreased in *Slc25a32*$^{-/-}$ embryos upon formate treatment, but they were still significantly higher when compared with the WT embryos. 12.5% of *Slc25a32*$^{-/-}$ embryos still had NTDs after formate supplementation, whose folate profiles were similar to the *Slc25a32*$^{-/-}$ embryos with NTDs before formate treatment.

These data proved that SLC25A32 was not involved in mitochondrial folate transport. However, *Slc25a32* mutations would interrupt folate metabolism, leading to mitochondrial folate deficiency or whole embryo CH3-THF shortage.

Slc25a32$^{-/-}$ mice embryos suffered from glycine cleavage defect due to deficiency in dihydrolipoamide dehydrogenase (DLDH)

Since formate supplementation successfully increased the CH3-THF levels and ameliorated the NTDs in *Slc25a32*$^{-/-}$ embryos, we wondered whether the *Slc25a32*$^{-/-}$ embryos suffered formate deficiency. We quantified the formate in whole embryos and found that the formate amounts in *Slc25a32*$^{-/-}$ embryos were about 70% of controls (Fig. 4A). Formate is an intermediate of one-carbon (1C) metabolism and is produced through the mitochondrial metabolism of metabolic substrates, including serine, glycine, sarcosine, and dimethylglycine (DMG) [11]. Analysis of these metabolic substrates in embryo homogenates showed that the *Slc25a32*$^{-/-}$ embryos had significantly increased glycine and serine contents, whereas *Slc25a32*$^{K235R/K235R}$ had significantly increased serine but significantly decreased glycine contents (Fig. 4B), when compared with WT embryos. There was no significant difference between *Slc25a32* mutant and WT embryos in sarcosine and DMG levels.

A more than threefold increase of glycine was specifically identified in the *Slc25a32*$^{-/-}$ embryos, which led us to hypothesize that formate deficiency found in *Slc25a32*$^{-/-}$ embryos resulted from glycine cleavage defect. To prove the hypothesis, we measured the mitochondria produced formate using a stable isotope-labeled [$^{13}C_2$]-glycine as the substrate. The amounts of [^{13}C]-formate produced by *Slc25a32*$^{-/-}$ embryo mitochondria was about 10.6% of controls (Fig. 4C), uncovering a causative role of glycine oxidation deficit in *Slc25a32*$^{-/-}$ embryos. We further measured the protein contents of the four subunits of glycine cleavage system (GCS). The results showed that the amounts of amino methyltransferase (AMT), glycine decarboxylase (GLDC), and hydrogen carrier protein (GCSH) in *Slc25a32*$^{-/-}$ embryos were comparable to that in WT embryos, but the amounts of DLDH were significantly lower in *Slc25a32*$^{-/-}$ embryos than in WT embryos (Fig. 4D). The enzymatic activity assay revealed that the mitochondrial DLDH activity in *Slc25a32*$^{-/-}$ was about 23.9% of controls (Fig. 4E). DLDH is an oxidoreductase in the mitochondrial matrix, and its activity is dependent on the presence of both FAD and NAD [31].

The *Slc25a32* mutations specifically blocked the mitochondrial uptake of FAD

SLC25A32 had been identified as a mitochondrial FAD transporter based on the experiment that transfection of the human *SLC25A32* gene functionally complemented the *FLX1* mutant yeast strain with mitochondrial FAD transport defect [6]. We then hypothesized that DLDH deficiency in *Slc25a32*$^{-/-}$ mitochondria resulted from the deprivation of FAD due to SLC25A32 dysfunction. Here, we first measured the mitochondrial contents of FAD and its precursors, FMN and Rf, in mitochondria. Compared with WT controls, the *Slc25a32*$^{Y174C/K235R}$ and *Slc25a32*$^{K235R/K235R}$ mice, but not the *Slc25a32*$^{Y174C/Y174C}$ mice, had significantly lower FAD, FMN, and/or Rf contents (Fig. 5A). The *Slc25a32*$^{-/-}$ embryos also suffered from mitochondrial FAD, FMN, and Rf shortages (Fig. 5B). By analyzing the mitochondrial uptake of stable isotope-labeled [$^{13}C_5$]-FAD

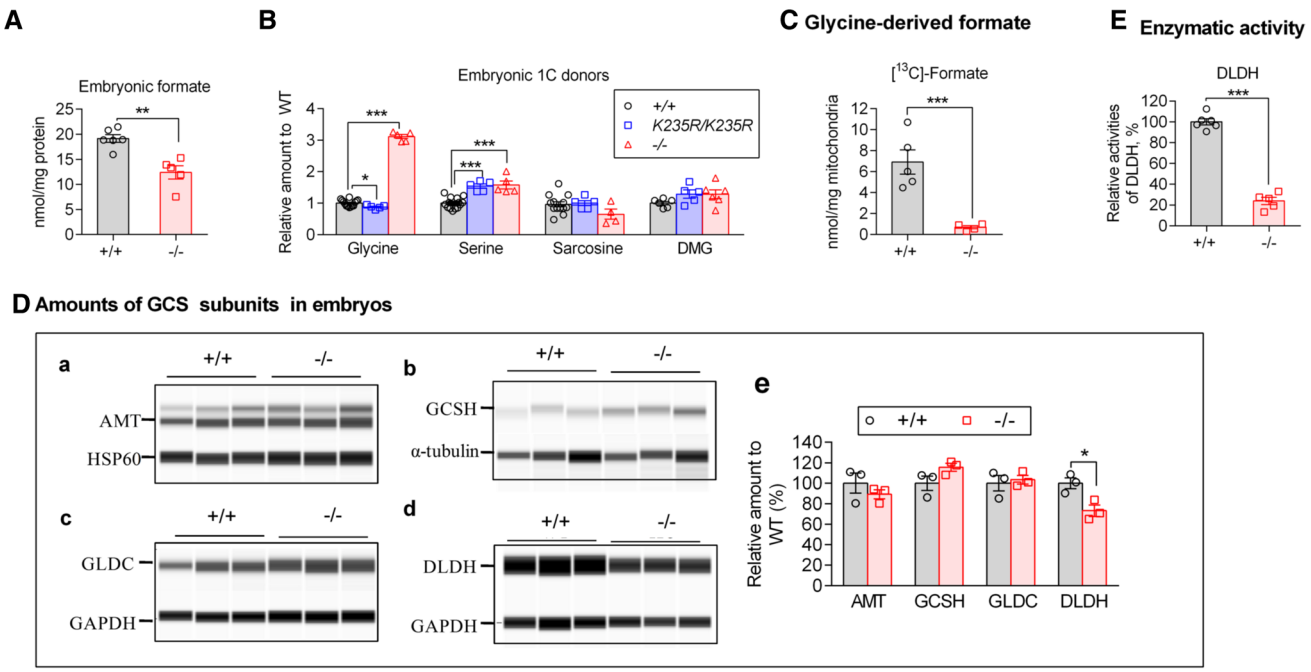

Fig. 4 Glycine cleavage defect was identified in *Slc25a32*$^{-/-}$ embryos. **A** Formate amounts in whole embryos ($n=5$–6). The *Slc25a32*$^{-/-}$ embryos had significantly lower amounts of formate than *Slc25a32*$^{+/+}$ embryos. **B** The contents of 1C donors in whole embryos ($n=4$–14). Significant differences in abundances between *Slc25a32*$^{K235R/K235R}$ and *Slc25a32*$^{+/+}$ embryos and between *Slc25a32*$^{-/-}$ and *Slc25a32*$^{+/+}$ embryos were noted for glycine and serine. **C** Isolated mitochondria produced [^{13}C]-formate amounts in 24 h using [1, 2-$^{13}C_2$]-glycine as substrate. A significant lower amount of [^{13}C]-formate was detected in *Slc25a32*$^{-/-}$ embryos than in *Slc25a32*$^{+/+}$ embryos. **D** Western blot analysis of four subunits of GCS in embryos (**a**–**d**, $n=3$). The relative abundance of each protein in *Slc25a32*$^{-/-}$ embryo was expressed as a ratio compared to the mean value of *Slc25a32*$^{+/+}$ embryos **e**. HSP60, α-tubulin, or GAPDH was used as a loading control for each subunit. The *Slc25a32*$^{-/-}$ embryos had significantly lower amounts of DLDH. **E** Enzymatic activity of DLDH ($n=5$–6). The activity of DLDH was significantly lower in *Slc25a32*$^{-/-}$ embryos than in *Slc25a32*$^{+/+}$ embryos. *n* represents biologically independent replicates. Data are mean ± SEM. *P* values were determined by an unpaired, two-tailed Student's *t* test. $*P<0.05$, $**P<0.01$, $***P<0.001$ versus *Slc25a32*$^{+/+}$ controls

and [$^{13}C_4$, $^{15}N_2$]-Rf, we found the *Slc25a32 K235R* mutation specifically blocked the mitochondria uptake of [$^{13}C_5$]-FAD, as indicated by the significantly lower uptake amounts of [$^{13}C_5$]-FAD in *Slc25a32*$^{Y174C/K235R}$ and *Slc25a32*$^{K235R/K235R}$ mitochondria, when compared with controls (Fig. 5C). Instead, *Slc25a32* mutations did not hinder the uptake of [$^{13}C_4$, $^{15}N_2$]-Rf, and the *Y174C* mutation even promoted the uptake of Rf, which suggested that the mitochondrial Rf deficiency in *Slc25a32* mutant mice derived from FAD shortage instead of Rf transport deficiency. Knock-out of *Slc25a32* also disabled the mitochondria from transporting [$^{13}C_5$]-FAD, as indicated by the low abundance of [$^{13}C_5$]-FAD in the mitochondria and high abundance of [$^{13}C_5$]-FAD in the incubation buffer of *Slc25a32*$^{-/-}$ embryos (Fig. 5D).

Slc25a32 mutations caused various degrees of damage to mitochondrial flavoenzymes.

Our data proved that the *Slc25a32* mutations affected the uptake of FAD into the mitochondria. FAD was a cofactor of multiple mitochondrial dehydrogenases involved in FAO, amino acids, and choline metabolisms [32]. By quantifying acylcarnitine levels, we found *Slc25a32*$^{-/-}$ embryos had MADD-like acylcarnitine profiles with significantly elevated levels of butyryl-, isobutyryl-, 2-methylbutyryl-, isovaleryl-, glutaryl-, hexanoyl-, octanoyl-, and stearoyl carnitine, and significantly decreased levels of free carnitine, acetyl-, propionyl-, 3-hydoxylbutyryl-, 3-hydroxylisovaleryl-, 3-hydroxylhexanoyl-, 3-hydroxyloctanoyl-, and 3-hydroxyldecanoyl carnitine, when compared with WT embryos (Fig. 6A). For the adult *Slc25a32* mutant mice, the *Slc25a32*$^{K235R/K235R}$ mice showed severe metabolic disturbance, *Slc25a32*$^{Y174C/K235R}$ mice had a mild one, and *Slc25a32*$^{Y174C/Y174C}$ mice had no disorder in muscle (Fig. 6B) and brain tissues (Fig. 6C), which revealed a positive correlation between FAD transport deficiency and metabolic disturbance. In addition, organ-specific involvement was observed. The *Slc25a32*$^{K235R/K235R}$ mice had the skeletal muscle and brain most severely affected, but the liver was less affected (data not shown). The *Slc25a32*$^{Y174C/K235R}$ mice had almost normal muscle acylcarnitine profiles, but abnormal brain

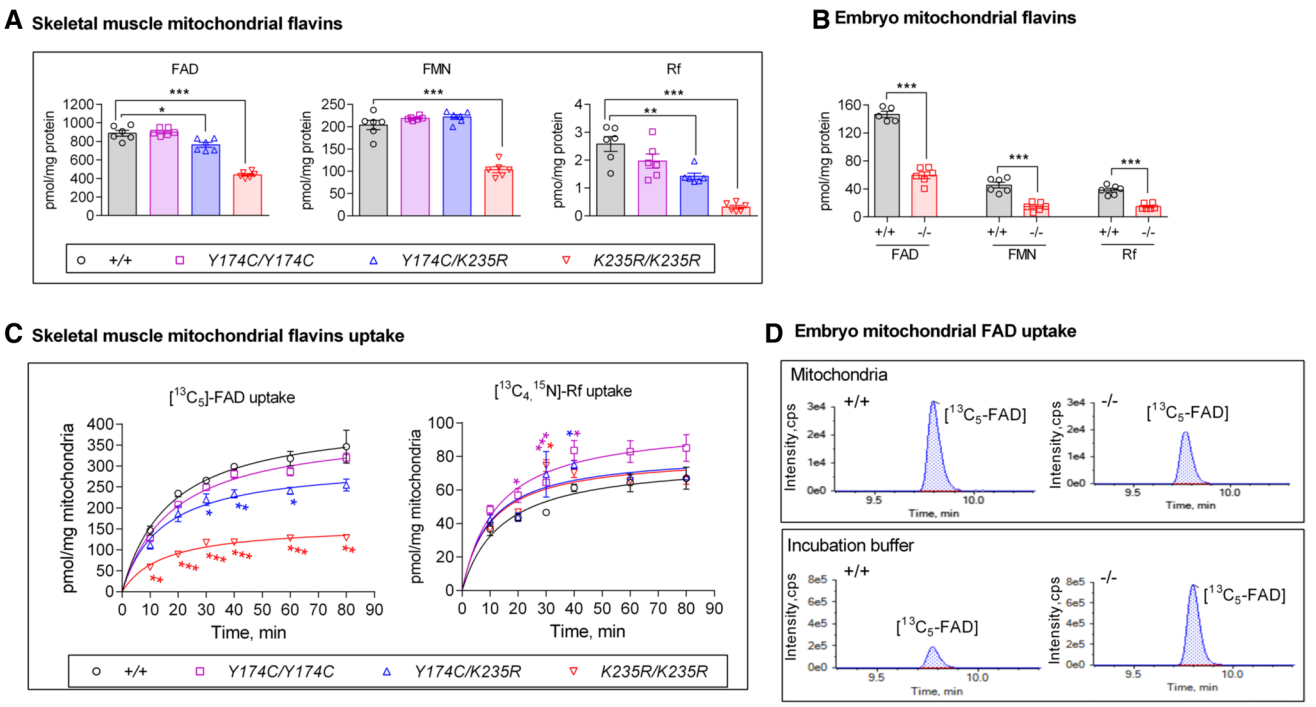

Fig. 5 *Slc25a32* mutations specifically affected the mitochondrial uptake of FAD. **A** The contents of flavins in mitochondria isolated from skeletal muscle of mice ($n=6$). Deficiencies of FAD, FMN, and Rf were observed in $Slc25a32^{Y174C/K235R}$ and $Slc25a32^{K235R/K235R}$ mice. **B** The contents of flavins in mitochondria isolated from embryos ($n=5$–6). Deficiencies of FAD, FMN, and Rf were observed in $Slc25a32^{-/-}$ embryos. **C** Mitochondria uptake of [$^{13}C_5$]-FAD and [$^{13}C_4$, $^{15}N_2$]-Rf ($n=3$). Mitochondria were isolated from the skeletal muscle of mice. Significantly lower [$^{13}C_5$]-FAD uptake rates were detected in $Slc25a32^{K235R/K235R}$ and $Slc25a32^{Y174C/K235R}$ mitochondria than in $Slc25a32^{+/+}$ mitochondria. **D** Mitochondria uptake of [$^{13}C_5$]-FAD. Mitochondria were isolated from embryos and incubated with 10 μmol/L [$^{13}C_5$]-FAD for 60 min. The LC–MS/MS TIC spectra revealed a low abundance of [$^{13}C_5$]-FAD in $Slc25a32^{-/-}$ mitochondria and a high abundance of [$^{13}C_5$]-FAD in $Slc25a32^{-/-}$ mitochondria incubation buffer. *n* represents biologically independent replicates. Data are mean ± SEM. *P* values were determined by an unpaired, two-tailed Student's *t* test. $^*P<0.05$, $^{**}P<0.01$, $^{***}P<0.001$ versus $Slc25a32^{+/+}$ controls

acylcarnitine profiles (Fig. 6B and C). Further analysis of organic acids and choline metabolites found glutaric acid and DMG accumulated in skeletal muscle and/or brain tissues of $Slc25a32^{K235R/K235R}$ and $Slc25a32^{Y174C/K235R}$ mice (Fig. 6D and E), which was consistent with the plasma biochemical profile of the patient. DMG is also an intermediate involved in mitochondrial formate generation. Quantifying formate contents showed significantly reduced formate contents in skeletal muscle lysates of $Slc25a32^{K235R/K235R}$ and $Slc25a32^{Y174C/K235R}$ mice (Fig. 6F).

SBCAD, IVD, IBD, and GCDH are flavoenzymes involved in the metabolism of leucine, isoleucine, valine, tryptophan, hydroxylysine, and lysine, and SCAD, MCAD, and VLCAD are flavoenzymes participating in FAO. The enzymatic activity assays confirmed lower activities of all these flavoenzymes in $Slc25a32^{K235R/K235R}$ mice than in WT controls (Fig. 7A–G). Decreased activities of GCDH and SCAD were also found in $Slc25a32^{Y174C/K235R}$ mice. FAD supplementation in vitro completely restored the function of SBCAD (Fig. 7A) and markedly increased the activities of IVD and GCDH (Fig. 7B and C), but only mildly improved the activities of SCAD, MCAD, VLCAD, and IBD (Fig. 7D-G) in $Slc25a32^{K235R/K235R}$ and $Slc25a32^{Y174C/K235R}$ mice. The immunoblot assays further revealed lower amounts of these flavoenzymes in $Slc25a32^{K235R/K235R}$ mice than in WT controls (Fig. 7H) and the reduction degrees correlated with their responses to FAD supplementation. We also measured the amounts of flavoenzymes involved in electron transportation and found that the amounts of ETFα, ETFβ, and ETFDH were lower in $Slc25a32^{K235R/K235R}$ mice than in controls (Fig. 7H).

Effect of riboflavin and formate supplementation on *Slc25a32* mutant mice

Since FAD could be synthesized from riboflavin in mitochondria [33], we tried riboflavin supplementation (1 g/kg riboflavin in diet) for $Slc25a32^{K235R/K235R}$ and $Slc25a32^{Y174C/K235R}$ mice. After 1 month of treatment, the mutant mice had no improvement in motor function. Further mitochondrial flavin analysis found no increase in riboflavin and FAD levels, suggesting that the orally supplemented

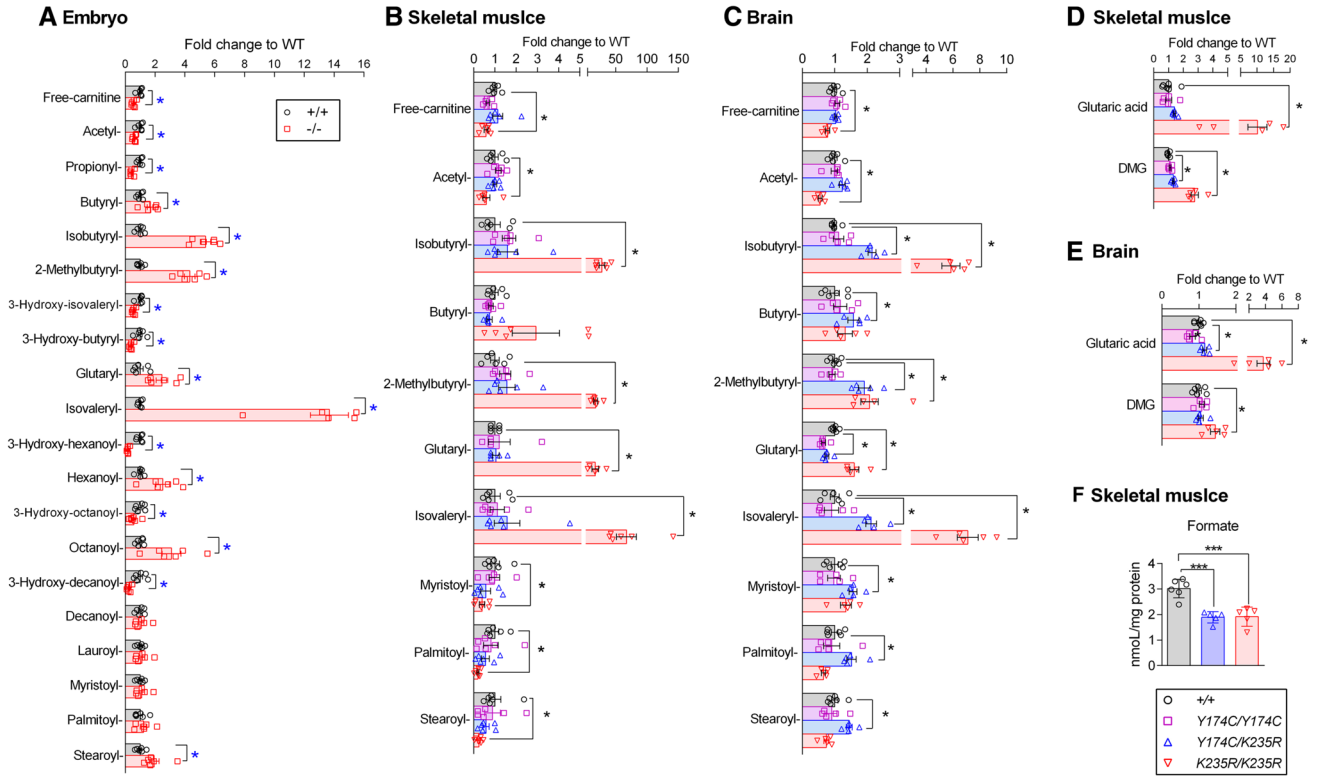

Fig. 6 *Slc25a32* mutant mice recapitulated the MADD-like biochemical features of the RREI patient. **A–C** Acylcarnitine profiles of embryos, skeletal muscle, and brain tissues of mice ($n=5$). Accumulation of multiple acylcarnitines and deficiency of free carnitine were found in *Slc25a32*$^{-/-}$ embryos, *Slc25a32*$^{K235R/K235R}$, and *Slc25a32*$^{Y174C/K235R}$ mice. **D–E** Glutaric acid and DMG amounts in skeletal muscle and brain tissues of *Slc25a32* mutant mice ($n=5$). Glutaric acid and DMG accumulated in *Slc25a32*$^{Y174C/K235R}$ and *Slc25a32*$^{K235R/K235R}$ mice tissues. **F** Quantification of formate contents in skeletal muscle lysates of mice ($n=5$). *Slc25a32*$^{K235R/K235R}$ and *Slc25a32*$^{Y174C/K235R}$ mice showed significantly reduced formate contents. *n* represents biologically independent replicates. Data are mean ± SEM. *P* values were determined by an unpaired, two-tailed Student's *t* test. $^{*}P<0.05$ versus *Slc25a32*$^{+/+}$ control

riboflavin had not been effectively absorbed by mice. Since the *Slc25a32* mutant mice suffered from mitochondrial folate shortage, we added 0.1 mol/L sodium formate to their drinking water to study whether formate could improve folate shortage. After a 3-week treatment, the WT mice had total folates increased from 5.33 ± 0.58 to 13.03 ± 0.41 pmol/mg protein, and *Slc25a32*$^{K235R/K235R}$ mice had total folates increased from 2.34 ± 0.70 to 6.08 ± 0.59 pmol/mg protein (Fig. 8). This folate elevation effect was not restricted to the *Slc25a32* mutant mice, and the disparity in folate amounts between *Slc25a32*$^{K235R/K235R}$ and WT mice still exist.

Discussion

In this work, we described a new case of RREI with *SLC25A32* missense mutations and generated several mice models to characterize the molecular mechanisms underlying *SLC25A32* mutations-induced RREI. Our study suggested that SLC25A32 was a mitochondrial FAD transporter instead of a folate transporter. SLC25A32 dysfunction blocked FAD entry into mitochondria and resulted in mitochondrial FAD deficiency. Two of the three mice models with *Slc25a32* missense mutations, one possessed homozygous K235R mutations, and the other had compound heterozygous Y174C/K235R mutations, presented with mild motor impairment, which was consistent with the phenotype of our patient. Homology modeling analysis predicted that K235 was located at the substrate-binding pocket. Consistent with the prediction, the homozygous K235R mutations profoundly affected mitochondrial FAD uptake, resulting in severe metabolic disturbance. Y174 was predicted to be located at the second matrix loop of the *Slc25a32* gene, facing the mitochondrial matrix. Homozygous Y174C mutation diminished *Slc25a32* mRNA and protein expression, but it did not cause a significant defect in mitochondrial FAD transport. The compound heterozygous Y174C/K235R mutations, which mimicked the mutations of our patient, led to mild mitochondrial FAD uptake deficiency and metabolic disturbance.

A positive correlation between SLC25A32 dysfunction and mitochondrial flavoenzymes defect was observed by

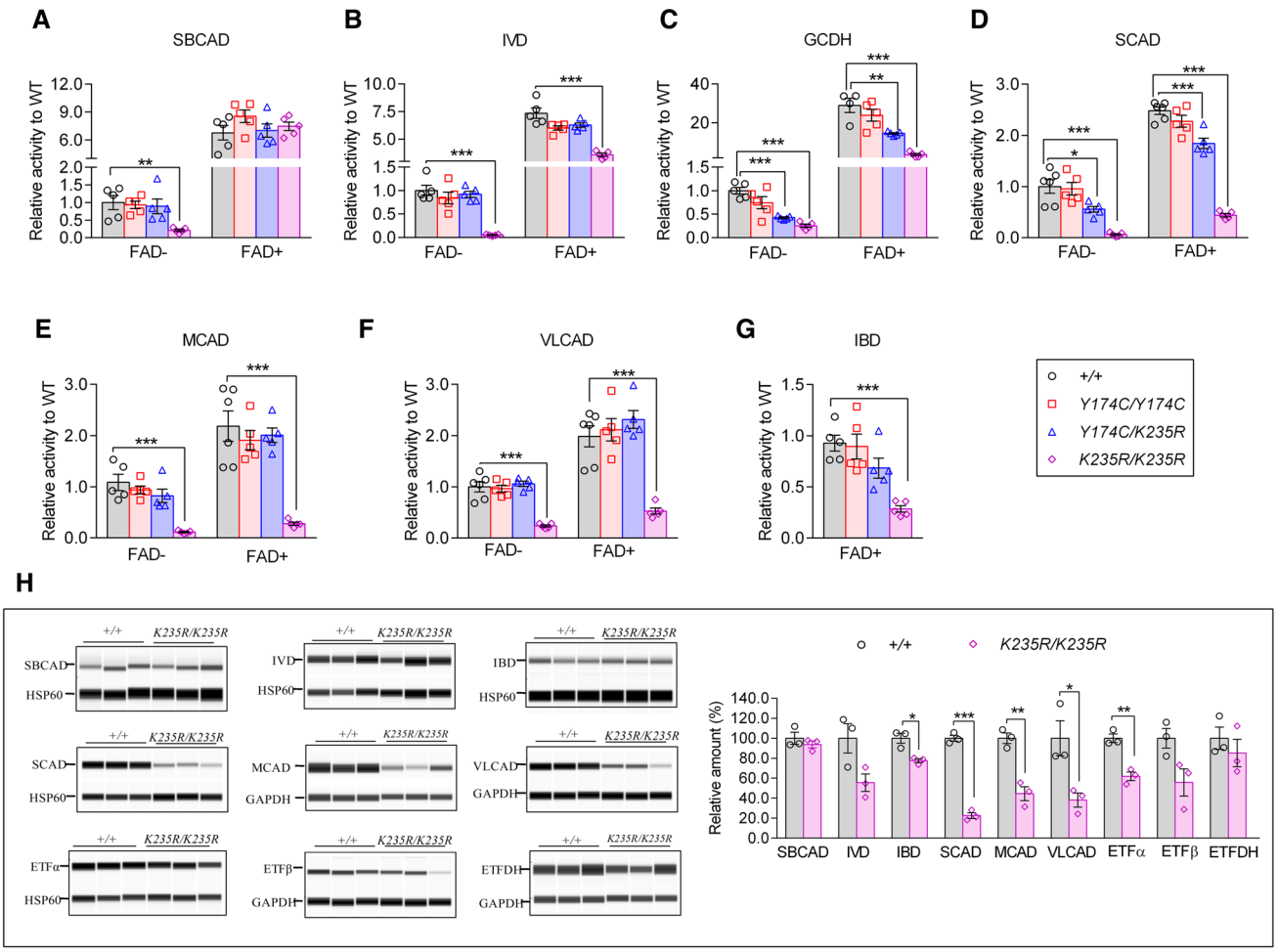

Fig. 7 *Slc25a32* mutations affect multiple mitochondrial flavoenzymes. **A–G** Enzymatic activities of muscular SBCAD, IVD, SCAD, MCAD, VLCAD, GCDH, and IBD, in the reaction system with or without FAD supplementation ($n=5$). Differences in activities between genotypes were noted for these enzymes. **I** Western blot analysis of nine mitochondrial flavoproteins in skeletal muscle tissues of $Slc25a32^{K235R/K235R}$ mice compared to $Slc25a32^{+/+}$ mice ($n=3$). HSP60 or GAPDH was used as a loading control for each protein. Significant differences in protein contents between genotypes were noted for IBD, SCAD, MCAD, VLCAD, and ETFα. *n* represents biologically independent replicates. Data are mean ± SEM. *P* values were determined by an unpaired, two-tailed Student's *t* test. $^{*}P<0.05$, $^{**}P<0.01$, $^{***}P<0.001$ versus $Slc25a32^{+/+}$ control

studying the three mice models simultaneously. FAD is a redox cofactor ensuring the function of many flavoenzymes involved in fundamental biochemical processes [32]. Given the central importance of FAD, it is reasonable to expect a large global change in metabolites upon mitochondrial FAD deficiency. As expected, the metabolic analysis demonstrated that multiple biochemical processes related to ATP generation, including FAO, catabolism of multiple essential amino acids (leucine, isoleucine, valine, tryptophan, lysine), and degradation of choline were interrupted by SLC25A32 dysfunction (Fig. 9). Furthermore, enzymatic activity and immunoblot assays confirmed the impairment of flavoenzymes involved in these oxidation processes and revealed that the electron transport chain was also affected. Moreover, we found that the SLC25A32 dysfunction differentially affected different flavoenzymes. For example, it abolished the conversion of apoprotein to holoprotein of SBCAD, resulting in exogenous FAD-rescuable function deficiency in vitro; it also diminished the amounts of flavoproteins involved in FAO, leading to exogenous FAD-irretrievable activity. The latter further confirmed the role of FAD in flavoprotein folding and cellular stability [34, 35]. This data explained the responses of plasma biochemical indicators of the patient to riboflavin supplementation: the indicators of SBCAD and IVD deficiencies, 2-methylbutyryl and isovaleryl carnitine, had levels normalized quickly, whereas the indicators of MCAD and VLCAD deficiencies, octanoyl- and myristoyl carnitine had the levels gradually normalized in more than 3 years.

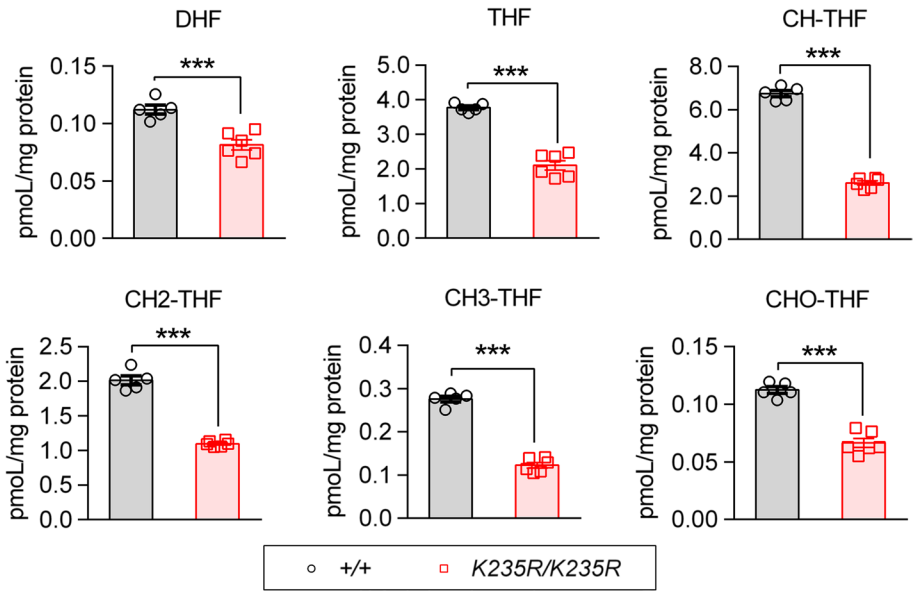

Fig. 8 Effect of formate supplementation on mitochondrial folate profile of *Slc25a32*$^{K235R/K235R}$ mice. The abundances of all folate intermediates were significantly lower in *Slc25a32*$^{K235R/K235R}$ mice than in *Slc25a32*$^{+/+}$ mice ($n=5$–6). *n* represents biologically independent replicates. Data are mean ± SEM. *P* values were determined by an unpaired, two-tailed Student's *t* test. ***$P<0.001$ versus *Slc25a32*$^{+/+}$ control

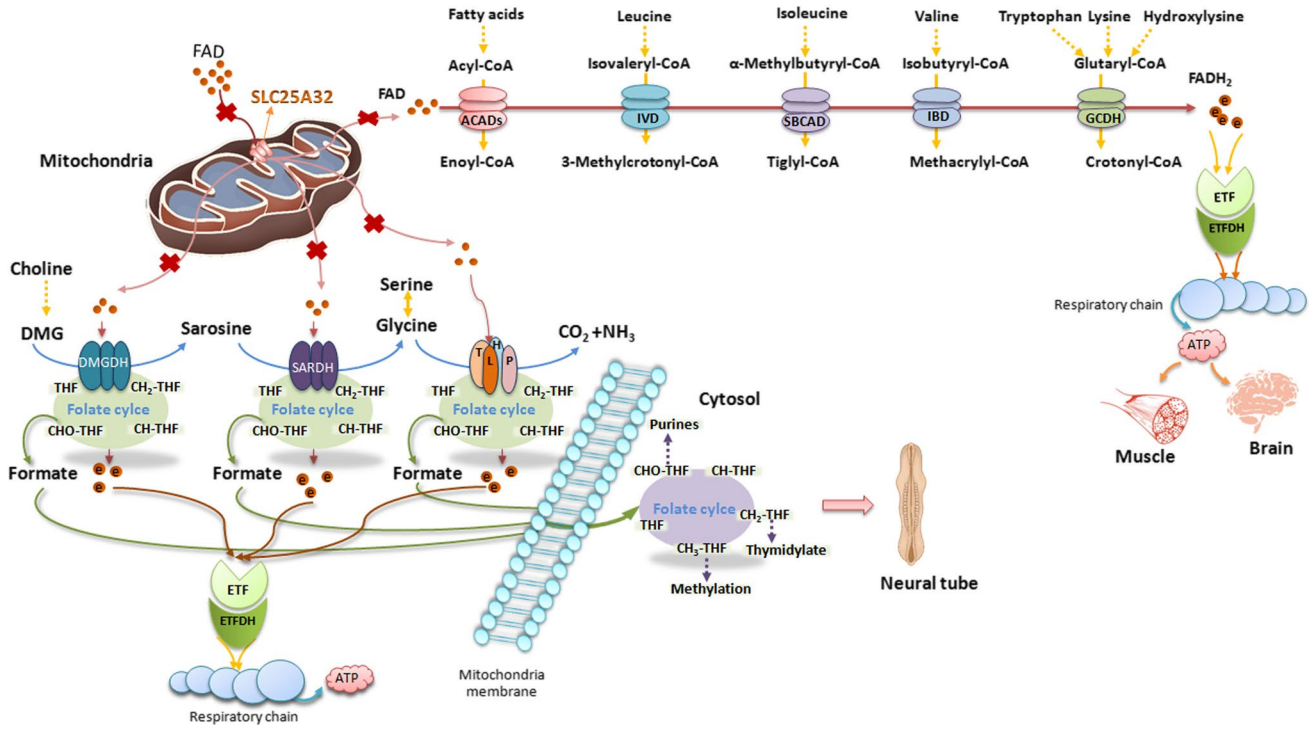

Fig. 9 Schematic diagram summarizing the principal metabolic pathways affected by SLC25A32 dysfunction. Enzymes involved in fatty acid *β*-oxidation, amino acids (glycine leucine, isoleucine, valine, tryptophan, lysine, and tryptophan) catabolism, and choline metabolism are FAD-dependent flavoproteins, which catalyze dehydrogenation reactions and transfer electrons to the mitochondrial respiratory chain through ETF and ETFDH sequentially. SLC25A32 dysfunction diminishes mitochondrial FAD contents, resulting in deficiencies of these metabolic pathways, which further affects ATP production and 1C unit generation, leading to impairment of muscle and brain function as well as neural tube closure

It has long been appreciated that SLC25A32 was a mammalian mitochondrial folate transporter [4, 7]. In this study, our *Slc25a32*$^{-/-}$ mice model presented with embryonic lethality and NTDs, which was consistent with the phenotype of *Slc25a32* gene-trapped mice [9]. Given the known importance of FOCM in neural tube closure, the NTDs in

the mice models suggested the involvement of FOCM in SLC25A32 dysfunction. By quantifying formate and all folate intermediate contents in embryo homogenates, we confirmed the disorder of FOCM in *Slc25a32*$^{-/-}$ embryo. However, the mitochondrial folate uptake assay disclosed the intact mitochondrial folate transport capacity in *Slc25a32*$^{-/-}$ embryo. Therefore, other factors should be considered as the cause of FOCM in *Slc25a32*$^{-/-}$ embryo. Analysis of 1C donors revealed glycine accumulation in *Slc25a32*$^{-/-}$ embryos. The glycine is the most critical 1C supplier in the neurulation stage of embryos [36]. It was oxidized to CO_2, NH_3, and a 1C unit in the form of CH2-THF (Fig. 9) under the function of strictly mitochondrial GCS. Glycine oxidation defects caused by dysfunctions of subunits of GCS, such as GLDC and AMT in humans and mice, had been evidenced with NTDs phenotype [37, 38]. Our study further proved significantly reduced formate generation from glycine in *Slc25a32*$^{-/-}$ embryo. Formate supplementation effectively increased the CH3-THF levels and ameliorated the NTDs in *Slc25a32*$^{-/-}$ embryos, suggesting that the underlying NTDs were due to a lack of 1C units derived from glycine. The discovery of DLDH deficiency was facilitated by measuring protein contents of the four subunits of GCS, which revealed the protein amount of DLDH instead of protein amounts of AMT, GLDC, and GCSH diminished in *Slc25a32*$^{-/-}$ embryos. SLC25A32 was a mitochondrial FAD transporter, according to our study. It was reasonable to propose that deletion of SLC25A32 made the FAD unavailable to DLDH, resulting in a deficiency of DLDH. Yeast with mitochondrial FAD transport defect also showed diminished activity of DLDH [39]. The correct folding of the DLDH depended on the presence of both FAD and NAD [31]. Previous studies have demonstrated that NAD deficiency inhibited the overall activity of GCS by competitive conjugation of apo-DLDH with other subunits of GCS [40]. In this study, the mildly decreased DLDH protein content (decreased 26.8%) and severely impaired GCS activity (reduced 89.4%) in *Slc25a32*$^{-/-}$ embryos suggested that FAD deficiency should have the same effect as NAD deficiency on GCS.

Unlike the *Slc25a32* knock-out mice embryos, the *Slc25a32* knock-in mice models had no glycine accumulation, suggesting glycine oxidation was unhindered. However, they also suffered from formate deficiency (Fig. 6F) and DMG accumulation (Fig. 6D, E). DMG is an intermediate of choline metabolism, which converts to sarcosine and donates 1C units to the folates cycle under the function of FAD-dependent dimethylglycine dehydrogenase (DMGDH) (Fig. 9) [41]. In addition to DMG, other 1C donors were also affected by *Slc25a32* missense mutations, as indicated by the elevated serine levels and decreased glycine levels in embryos (Fig. 4B). Moreover, high serine levels were also found in the adult *Slc25a32*$^{Y174C/K235R}$ mice brain ($(14.39 \pm 0.65$ *vs.* $16.64 \pm 0.50)$ pmol/mg protein, WT *vs.* *Slc25a32*$^{Y174C/K235R}$). The elevated serine and decreased glycine were probably due to an enhanced de novo synthesis of serine from the glycolytic intermediate 3-phosphoglycerate and enhanced utilization of glycine oxidation as an adaptive response to increase 1C donors [42]. The variation of glycine and serine in *Slc25a32* knock-in mice embryos was similar to that in methylenetetrahydrofolate dehydrogenase 1-like gene (*Mthfd1l*)-null mice embryos [42], suggesting mitochondrial folate metabolism was affected in *Slc25a32* knock-in mice. Quantification of folate intermediates confirmed the absence of mitochondrial folates (Fig. 3A). The data was consistent with the results obtained from glycine auxotrophy CHO-derived *glyB* cells [43] which possessed a G192E mutation in the *SLC25A32* gene [7]. Mitochondrial folate deficiency might be caused by inhibition of folate production, enhancement of folate removal rate, or less efficient folate utilization [43]. A recent study disclosed that ablating formate generation in mitochondria resulted in folate degradation [44]. Therefore, it is very likely that the *Slc25a32* missense mutations interrupted the choline metabolism, leading to a reduction of formate generation, which further enhanced folate removal and resulted in mitochondrial folate deficiency. Experiments to test this hypothesis are underway.

The relationships between mitochondrial folate deficiency and phenotypes of patients with RREI remain undefined. The mice models did not reproduce the phenotypes of clubfoot, fibulae hypoplasia, and lateral ventricle enlargement of our patient. However, previous studies already revealed a strong link between folate deficiency and clubfoot and ventriculomegaly in humans [45–49], which provided insights into the cause of clubfeet in our patient. In fact, the etiopathogenesis of congenital clubfoot is still unknown regardless of its long-lasting recognition. More recently, the clubfoot was proposed to be caused by a defect of both the radial and the longitudinal growth unevenly affecting the leg muscles with a consequent imbalance of the foot activators [50]. Interestingly, folate was found to play roles in skeletal muscle cell development and function [51].

Mitochondrial FAD deficiency could be caused not only by SLC25A32 dysfunction, but also by other inborn errors, such as electron transportation defects [52], riboflavin transport disorders [53], and FAD synthase deficiency [54]. Since SLC25A32 dysfunction-caused mitochondrial FAD deficiency resulted in folate shortage, other inborn errors would also cause similar metabolic abnormalities. Therefore, it is valuable to clarify the role of folate shortage in the morphological change of humans.

As summarized in Fig. 9, our study demonstrated that SLC25A32 was a mitochondrial FAD transporter instead of a folate transporter. SLC25A32 dysfunction blocked FAD entry into mitochondria, resulting in mitochondrial FAD shortage and impairment of mitochondrial acyl-CoA

dehydrogenases and electron transfer chain, which further damaged muscle and brain function. SLC25A32 dysfunction also disrupted FOCM by diminishing the generation of 1C unit from mitochondria, leading to NTDs in embryos.

Acknowledgements We warmly thank the patient and her parents for participating in this study. We also thank Zhu-Yuan Xu (Account Manager, ProteinSimple) and Zu-Sen Weng (FAS, ProteinSimple) for their help in the Western blot assays, Zhe Li (Ph.D, School of Pharmaceutical Sciences, Sun Yat-sen University) for his help in the homology modeling analysis, and Prof. Ya-Ping Tang (Guangzhou Women and Children's Medical Center) and Prof. Guo-Jun Shi (The third affiliated hospital, Sun-Yat Sen University) for their valuable suggestions in preparing the manuscript.

Author contributions Study concept and design were undertaken by M-Z P, Y-X S, and L L. Data acquisition and analysis were undertaken by M-Z P, Y-X S, X-Z L, K-D Z, Y-N C, Y-T L, M-Y J, Z-C L, X-Y S, W Z, and X-L J. The manuscript was written by M-Z P. and revised by L L, Y-X S, and X-L J.

Funding This study was funded by the National Natural Science Foundation of China (81802125 to M-Z P., 81700755 to Y-X S., and 81873661 to L L.), and Guangzhou Women and Children's Medical Center/Guangzhou Institute of Pediatrics (IP-2018-024 to M-Z P.). The funding sources are not involved with the preparation of the article.

Data availability The datasets generated during or analyzed during the current study are all available in the manuscript.

Declarations

Conflict of interest The authors have no conflict of interest to declare.

Ethical approval and consent to participate This study was performed in line with the principles of the Declaration of Helsinki. The ethics committee of Guangzhou Women and Children's Medical Center authorized this study, and the Institutional Animal Care and Use Committee of Guangzhou Medical University approved the animal studies. Informed consent has been obtained from the patient and her guardian.

Consent for publication The authors affirm that human research participants provided informed consent for publication of the images in Fig. 1b, 1c and 1d.

References

1. Schiff M, Veauville-Merllié A, Su CH et al (2016) SLC25A32 mutations and riboflavin-responsive exercise intolerance. N Engl J Med. https://doi.org/10.1056/NEJMc1513610
2. Hellebrekers DMEI, Sallevelt SCEH, Theunissen TEJ et al (2017) Novel SLC25A32 mutation in a patient with a severe neuromuscular phenotype. Eur J Hum Genet. https://doi.org/10.1038/ejhg.2017.62
3. Al Shamsi B, Al Murshedi F, Al Habsi A, Al-Thihli K (2021) Hypoketotic hypoglycemia without neuromuscular complications in patients with slc25a32 deficiency. Eur J Hum Genet. https://doi.org/10.1038/s41431-021-00995-7
4. Titus SA, Moran RG (2000) Retrovirally mediated complementation of the glyb phenotype: cloning of a human gene encoding the carrier for entry of folates into mitochondria. J Biol Chem. https://doi.org/10.1074/jbc.M005163200
5. Haitina T, Lindblom J, Renström T, Fredriksson R (2006) Fourteen novel human members of mitochondrial solute carrier family 25 (SLC25) widely expressed in the central nervous system. Genomics. https://doi.org/10.1016/j.ygeno.2006.06.016
6. Spaan AN, Ijlst L, van Roermund CWT et al (2005) Identification of the human mitochondrial FAD transporter and its potential role in multiple acyl-coa dehydrogenase deficiency. Mol Genet Metab. https://doi.org/10.1016/j.ymgme.2005.07.014;86:441-7
7. McCarthy EA, Titus SA, Taylor SM et al (2004) A mutation inactivating the mitochondrial inner membrane folate transporter creates a glycine requirement for survival of Chinese hamster cells. J Biol Chem. https://doi.org/10.1074/jbc.M403677200
8. Becker ML, van Haandel L, Gaedigk R et al (2012) Red blood cell folate concentrations and polyglutamate distribution in juvenile arthritis: predictors of folate variability. Pharmacogenet Genomics. https://doi.org/10.1097/FPC.0b013e3283500202
9. Kim J, Lei Y, Guo J et al (2018) Formate rescues neural tube defects caused by mutations in slc25a32. Proc Natl Acad Sci USA. https://doi.org/10.1073/pnas.1800138115
10. Steele JW, Kim SE, Finnell RH (2020) One-carbon metabolism and folate transporter genes: do they factor prominently in the genetic etiology of neural tube defects? Biochimie. https://doi.org/10.1016/j.biochi.2020.02.005
11. Ducker GS, Rabinowitz JD (2017) One-carbon metabolism in health and disease. Cell Metab. https://doi.org/10.1016/j.cmet.2016.08.009
12. Pavone V, Chisari E, Vescio A et al (2018) The etiology of idiopathic congenital talipes equinovarus: a systematic review. J Orthop Surg Res. https://doi.org/10.1186/s13018-018-0913-z
13. Frerman FE, Goodman SI (2019) Defects of electron transfer flavoprotein and electron transfer flavoprotein-ubiquinone oxidoreductase: glutaric acidemia type II. In: Valle DL, Antonarakis S, Ballabio A et al (eds) The online metabolic and molecular bases of inherited disease. McGraw Hill, New York
14. Frezza C, Cipolat S, Scorrano L (2007) Organelle isolation: functional mitochondria from mouse liver, muscle and cultured fibroblasts. Nat Protoc. https://doi.org/10.1038/nprot.2006.478
15. Chaiyarit S, Thongboonkerd V (2009) Comparative analyses of cell disruption methods for mitochondrial isolation in high-throughput proteomics study. Anal Biochem. https://doi.org/10.1016/j.ab.2009.07.026
16. Luongo TS, Eller JM, Lu MJ et al (2020) SLC25A51 is a mammalian mitochondrial NAD^+ transporter. Nature. https://doi.org/10.1038/s41586-020-2741-7
17. Leung K-Y, De Castro SCP, Cabreiro F et al (2013) Folate metabolite profiling of different cell types and embryos suggests variation in folate one-carbon metabolism, including developmental changes in human embryonic brain. Mol Cell Biochem. https://doi.org/10.1007/s11010-013-1613-y
18. Liu H, Xu F, Gao Y et al (2020) An integrated LC-MS/MS strategy for quantifying the oxidative-redox metabolome in multiple biological samples. Anal Chem. https://doi.org/10.1021/acs.analchem.0c00242
19. Peng M, Fang X, Huang Y et al (2013) Separation and identification of underivatized plasma acylcarnitine isomers using liquid chromatography–tandem mass spectrometry for the differential diagnosis of organic acidemias and fatty acid oxidation defects. J Chromatogr A. https://doi.org/10.1016/j.chroma.2013.10.036
20. Peng M-Z, Cai Y-N, Shao Y-X et al (2019) Simultaneous quantification of 48 plasma amino acids by liquid chromatography-tandem

mass spectrometry to investigate urea cycle disorders. Clin Chim Acta. https://doi.org/10.1016/j.cca.2019.05.011
21. Tan B, Lu Z, Dong S et al (2014) Derivatization of the tricarboxylic acid intermediates with o-benzylhydroxylamine for liquid chromatography–tandem mass spectrometry detection. Anal Biochem. https://doi.org/10.1016/j.ab.2014.07.027
22. Kirsch SH, Herrmann W, Rabagny Y, Obeid R (2010) Quantification of acetylcholine, choline, betaine, and dimethylglycine in human plasma and urine using stable-isotope dilution ultra performance liquid chromatography–tandem mass spectrometry. J Chromatogr B. https://doi.org/10.1016/j.jchromb.2010.10.016
23. Lamarre SG, MacMillan L, Morrow GP et al (2014) An isotope-dilution, GC–MS assay for formate and its application to human and animal metabolism. Amino Acids. https://doi.org/10.1007/s00726-014-1738-7
24. Tajima G, Sakura N, Yofune H et al (2005) Establishment of a practical enzymatic assay method for determination of isovaleryl-CoA dehydrogenase activity using high-performance liquid chromatography. Clin Chim Acta. https://doi.org/10.1016/j.cccn.2004.11.007
25. Bouvier D, Vianey-Saban C, Ruet S et al (2017) Development of a tandem mass spectrometry method for rapid measurement of medium- and very-long-chain acyl-CoA dehydrogenase activity in fibroblasts. In: Morava E, Baumgartner M, Patterson M, Rahman S, Zschocke J, Peters V (eds) JIMD Reports. Springer, Berlin, pp 71–78
26. Kerr D, Grahame G, Nakouzi G (2012) Assays of pyruvate dehydrogenase complex and pyruvate carboxylase activity. Methods Mol Biol. https://doi.org/10.1007/978-1-61779-504-6_7
27. Morrow GP, MacMillan L, Lamarre SG et al (2015) In vivo kinetics of formate metabolism in folate-deficient and folate-replete rats. J Biol Chem. https://doi.org/10.1074/jbc.M114.600718
28. Aartsma-Rus A, van Putten M (2014) Assessing functional performance in the mdx mouse model. J Vis Exp. https://doi.org/10.3791/51303
29. Brooks SP, Trueman RC, Dunnett SB (2012) Assessment of motor coordination and balance in mice using the rotarod, elevated bridge, and footprint tests. Curr Protoc Mouse Biol. https://doi.org/10.1002/9780470942390.mo110165
30. Lin C-Y, Jhang Y-S, Lai S-C et al (2017) Antifatigue properties of tanshinone iia in mice subjected to the forced swimming test. Pharm Biol. https://doi.org/10.1080/13880209.2017.1401648
31. Brautigam CA, Chuang JL, Tomchick DR et al (2005) Crystal structure of human dihydrolipoamide dehydrogenase: NAD+/NADH binding and the structural basis of disease-causing mutations. J Mol Biol. https://doi.org/10.1016/j.jmb.2005.05.014
32. Lienhart W-D, Gudipati V, Macheroux P (2013) The human flavoproteome. Arch Biochem Biophys. https://doi.org/10.1016/j.abb.2013.02.015
33. Barile M, Passarella S, Bertoldi A et al (1993) Flavin adenine dinucleotide synthesis in isolated rat liver mitochondria caused by imported flavin mononucleotide. Arch Biochem Biophys. https://doi.org/10.1006/abbi.1993.1444
34. Saijo T, Tanaka K (1995) Isoalloxazine ring of FAD is required for the formation of the core in the Hsp60-assisted folding of medium chain acyl-CoA dehydrogenase subunit into the assembly competent conformation in mitochondria. J Biol Chem. https://doi.org/10.1074/jbc.270.4.1899
35. Nagao M, Tanaka K (1992) FAD-dependent regulation of transcription, translation, post-translational processing, and post-processing stability of various mitochondrial acyl-CoA dehydrogenases and of electron transfer flavoprotein and the site of holoenzyme formation. J Biol Chem 267(25):17925–17932
36. Leung K-Y, Pai YJ, Chen Q et al (2017) Partitioning of one-carbon units in folate and methionine metabolism is essential for neural tube closure. Cell Rep. https://doi.org/10.1016/j.celrep.2017.10.072
37. Narisawa A, Komatsuzaki S, Kikuchi A et al (2012) Mutations in genes encoding the glycine cleavage system predispose to neural tube defects in mice and humans. Hum Mol Genet. https://doi.org/10.1093/hmg/ddr585
38. Pai YJ, Leung K-Y, Savery D et al (2015) Glycine decarboxylase deficiency causes neural tube defects and features of non-ketotic hyperglycinemia in mice. Nat Commun. https://doi.org/10.1038/ncomms7388
39. Tzagoloff A, Jang J, Glerum DM, Wu M (1996) FLX1 codes for a carrier protein involved in maintaining a proper balance of flavin nucleotides in yeast mitochondria. J Biol Chem. https://doi.org/10.1074/jbc.271.13.7392
40. Zhang X, Li M, Xu Y et al (2019) Quantitative study of H protein lipoylation of the glycine cleavage system and a strategy to increase its activity by co-expression of LplA. J Biol Eng. https://doi.org/10.1186/s13036-019-0164-5
41. Tibbetts AS, Appling DR (2010) Compartmentalization of mammalian folate-mediated one-carbon metabolism. Annu Rev Nutr. https://doi.org/10.1146/annurev.nutr.012809.104810
42. Bryant JD, Sweeney SR, Sentandreu E et al (2018) Deletion of the neural tube defect-associated gene Mthfd1l disrupts one-carbon and central energy metabolism in mouse embryos. J Biol Chem. https://doi.org/10.1074/jbc.RA118.002180
43. Kao F, Chasin L, Puck TT (1969) Genetics of somatic mammalian cells X Complementation analysis of glycine-requiring mutants. Proc Natl Acad Sci USA. https://doi.org/10.1073/pnas.64.4.1284
44. Zheng Y, Lin TY, Lee G et al (2018) Mitochondrial one-carbon pathway supports cytosolic folate integrity in cancer cells. Cell. https://doi.org/10.1016/j.cell.2018.09.041
45. Ulrich M, Kristoffersen K, Rolschau J et al (1999) The influence of folic acid supplement on the outcome of pregnancies in the county of Funen in Denmark. Part ii. Congenital anomalies. A randomised study. Eur J Obstet Gynecol Reprod Biol. https://doi.org/10.1016/S0301-2115(99)00085-8
46. Sharp L, Miedzybrodzka Z, Cardy AH et al (2006) The C677T polymorphism in the methylenetetrahydrofolate reductase gene (MTHFR), maternal use of folic acid supplements, and risk of isolated clubfoot: a case-parent-triad analysis. Am J Epidemiol. https://doi.org/10.1093/aje/kwj285
47. Overholser MD, Whitley JR, O'Dell BL, Hogan AG (1954) The ventricular system in hydrocephalic rat brains produced by a deficiency of vitamin B12 or of folic acid in the maternal diet. Anat Rec. https://doi.org/10.1002/ar.1091200407
48. Woodard JC, Newberne PM (1966) Relation of vitamin B12 and one-carbon metabolism to hydrocephalus in the rat. J Nutr. https://doi.org/10.1093/jn/88.4.375
49. Santos C, Pai YJ, Mahmood MR et al (2020) Impaired folate 1-carbon metabolism causes formate-preventable hydrocephalus in glycine decarboxylase-deficient mice. J Clin Investig. https://doi.org/10.1172/jci132360
50. Ippolito E, Gorgolini G (2021) Clubfoot pathology in fetus and pathogenesis. A new pathogenetic theory based on pathology, imaging findings and biomechanics-a narrative review. Ann Transl Med. 9(13):1095–1095
51. Hwang SY, Sung B, Kim ND (2019) Roles of folate in skeletal muscle cell development and functions. Arch Pharm Res. https://doi.org/10.1007/s12272-018-1100-9
52. Olsen RKJ, Olpin SE, Andresen BS et al (2007) ETFDH mutations as a major cause of riboflavin-responsive multiple acyl-CoA dehydrogenation deficiency. Brain. https://doi.org/10.1093/brain/awm135

53. O'Callaghan B, Bosch AM, Houlden H (2019) An update on the genetics, clinical presentation, and pathomechanisms of human riboflavin transporter deficiency. J Inherit Metab Dis. https://doi.org/10.1002/jimd.12053
54. Olsen RKJ, Koňaříková E, Giancaspero TA et al (2016) Riboflavin-responsive and -non-responsive mutations in fad synthase cause multiple acyl-CoA dehydrogenase and combined respiratory-chain deficiency. Am J Hum Genet. https://doi.org/10.1016/j.ajhg.2016.04.006